

*Annual Review of Nuclear and Particle Science*

# Physics of the Top Quark at the LHC: An Appraisal and Outlook of the Road Ahead

P. Ferreira da Silva

CERN, Genève, Switzerland; email: [psilva@cern.ch](mailto:psilva@cern.ch)

Annu. Rev. Nucl. Part. Sci. 2023. 73:255–84

The *Annual Review of Nuclear and Particle Science* is online at [nucl.annualreviews.org](http://nucl.annualreviews.org)

<https://doi.org/10.1146/annurev-nucl-102419-052854>

Copyright © 2023 by the author(s). This work is licensed under a Creative Commons Attribution 4.0 International License, which permits unrestricted use, distribution, and reproduction in any medium, provided the original author and source are credited. See credit lines of images or other third-party material in this article for license information.

ANNUAL  
REVIEWS **CONNECT**

[www.annualreviews.org](http://www.annualreviews.org)

- Download figures
- Navigate cited references
- Keyword search
- Explore related articles
- Share via email or social media

## Keywords

hadron collider, top quark, Standard Model, cross section, strong interactions, electroweak interactions, Higgs boson, beyond the Standard Model

## Abstract

Since its start, the Large Hadron Collider (LHC) has helped advance both theory and experiment on the production and properties of the heaviest fundamental particle, the top quark. This review focuses on a selected set of measurements and associated searches for new physics, which have opened the door for unprecedented precision in this area of high-energy physics. Fundamental parameters of the theory such as  $m_t$ ,  $\alpha_S$ ,  $V_{tb}$ , and  $y_t$  are measured from top quark events with relative uncertainties that are smaller than 0.5%, 1.8%, 2%, and 10%, respectively, and that are expected to improve with more data, better experimental methods, and more accurate theory predictions. Several results, even if statistically limited, already significantly constrain the phase space of new physics: measurements of associated production with bosons, processes with four top quarks, and searches for rare decays, among others. It is expected that until the completion of the LHC program, top quark physics will keep providing unique insights regarding the consistency of the Standard Model and the energy scale of new physics.

## Contents

1. INTRODUCTION .....	256
2. CHALLENGES IN TOP QUARK PHYSICS .....	257
2.1. What Is a Top Quark? .....	257
2.2. Modeling Limitations or Discoveries? .....	259
2.3. Pushing the Detector Frontier .....	259
3. TOP QUARK PRODUCTION AT THE LHC .....	261
3.1. Top Quark Pair Production .....	261
3.2. Single Top Quark Production .....	266
3.3. Associated Production of Top Quarks and Bosons .....	269
3.4. Associated Production with Heavy Flavors .....	271
3.5. Four Top Quark Production .....	272
3.6. Overview of Top Quark Production at the LHC .....	273
4. TOWARD THE DISCOVERY OF NEW PHYSICS THROUGH THE TOP QUARK FRONTIER .....	273
4.1. Projecting the Scale of New Physics From Current Measurements .....	274
4.2. Chasing the BSM Tail From Asymmetries in the Data .....	276
4.3. Probing Flavor-Related Anomalies with Top Quarks .....	277
5. SUMMARY AND OUTLOOK .....	278

## 1. INTRODUCTION

Exploration of the top quark sector provides a rich setup for testing the Standard Model of particle physics (SM). The physics of the electroweak (EW) interaction, quantum chromodynamics (QCD), and the Higgs boson blend in the production and decay of the top quark in particle colliders. The top quark's special role in the SM stems from having a very small mixing with quarks other than the bottom quark and a mass that is approximately 2.1 times that of a  $W$  boson and approximately 1.4 times that of a Higgs boson, making it the heaviest of the known elementary particles (1). These characteristics isolate the top quark within its particle family and grant it a privileged part in the radiative corrections to the Higgs mass, in constraining the space allowed from new physics contributions to the EW oblique parameters (2), and in directly influencing the stability of the weak scale (3). As such, measurements of top quark production and its properties have the potential to accurately test the SM by providing measurements of fundamental parameters of this theory. Moreover, many extensions of the SM predict new interactions with the top quark sector (4).

The ATLAS (5), CMS (6), and LHCb (7) experiments at the CERN Large Hadron Collider (LHC) have been exploring different aspects of top quark physics since 2010, inheriting the legacy of the top quark discovery and the first measurements performed by the CDF (8) and D0 (9) Collaborations at the Fermilab Tevatron. On several fronts, the precision attained has surpassed the theoretical one, opening the door for more stringent tests of the SM and higher sensitivity to new physics phenomena.

In this review, I focus on a selected set of the latest published results from the LHC experiments to highlight the challenges and road ahead for top quark physics toward the high-integrated-luminosity regime of the LHC. Clearly, such a selection entails a personal perspective; for other perspectives, the interested reader is invited to consult other recent extensive reviews including the historical perspectives in References 10–12 as well as the lists of all the available results on the

public web pages of the LHC collaborations (13–15) and the LHC Top Physics Working Group (LHCTopWG) (16).

This review is organized as follows. It begins by identifying the current challenges of top quark physics in Section 2. A more detailed overview of different production modes at the LHC is given in Section 3, and a brief discussion of the status and prospects of using top quark physics to find physics beyond the SM (BSM) at the LHC is presented in Section 4. An outlook is given in the final section.

## 2. CHALLENGES IN TOP QUARK PHYSICS

The successful exploration of the top quark sector in hadron colliders faces both theoretical and experimental challenges. Three main fronts are summarized in the following subsections.

### 2.1. What Is a Top Quark?

A top quark cannot be observed directly as it is a QCD color triplet with a very short lifetime:  $\tau_t = \hbar/\Gamma_t \approx 0.5 \times 10^{-24}$  s. Its natural width ( $\Gamma_t$ ) is intrinsically related to its mass ( $m_t$ ) and that of the  $W$  boson ( $m_W$ ) given that  $t \rightarrow Wb$  is, by far, the dominant decay channel:

$$\Gamma_t = \frac{G_F m_t^3}{8\pi\sqrt{2}} \left(1 - \frac{m_W^2}{m_t^2}\right)^2 \left(1 + 2\frac{m_W^2}{m_t^2}\right) \left[1 - \frac{2\alpha_S}{3\pi} \left(\frac{2\pi^2}{3} - \frac{5}{2}\right)\right] \approx 1.35 \text{ GeV}. \quad 1.$$

The final-state products comprise the decay products of a  $W$  boson and a  $b$  jet, given the dominance of the  $V_{tb}$  element of the CKM (Cabibbo–Kobayashi–Maskawa) matrix. The large value of  $m_t = 173.3$  GeV (17) and the dominance of a single decay channel to  $\Gamma_t$  set a natural time scale that provides a unique window for experimentally studying a “naked” quark (18). Any spin effect present at production is inherited by the decay products without being affected by hadronization, which occurs at a scale  $\Lambda_{\text{QCD}} \sim 200$  MeV, or by soft QCD depolarizing effects. In approximate terms, one has the following:

$$\underbrace{\frac{1}{m_t}}_{\substack{\text{Production} \\ 10^{-27} \text{ s}}} < \underbrace{\frac{1}{\Gamma_t}}_{\substack{\text{Decay} \\ 10^{-25} \text{ s}}} < \underbrace{\frac{1}{\Lambda_{\text{QCD}}}}_{\substack{\text{Hadronization} \\ 10^{-24} \text{ s}}} < \underbrace{\frac{m_t}{\Lambda_{\text{QCD}}}}_{\substack{\text{Spin flip} \\ 10^{-21} \text{ s}}}. \quad 2.$$

From observation of the decay products, one can therefore infer the initial kinematics and properties, given that  $\tau_t$  is shorter than both the hadronization and the spin-decorrelation time scales.

The reconstruction of the top quark from its decay products leads to an effective particle-level definition that Monte Carlo (MC) simulations can mimic. This experimentally driven definition is typically robust in its extrapolation to the full phase space of production (i.e., beyond detector acceptance) with respect to modeling effects and uncertainties. The particle-level definition suffers, however, from the dependency on the algorithm employed and from being an entity that cannot be used directly in comparisons with fixed-order calculations that make use of the notion of a parton-level top quark. This is often a limiting factor for measurements of fundamental parameters of the SM.

Although state-of-the-art MC simulations take into account several important effects summarized in Section 2.2 below, they have typically large uncertainties arising from being fixed-order in perturbation theory and from the parton shower (PS) generator used to evolve a parton to a jet of particles in the final state. An illustration of the several effects modeled by MC simulation is shown in **Figure 1**.

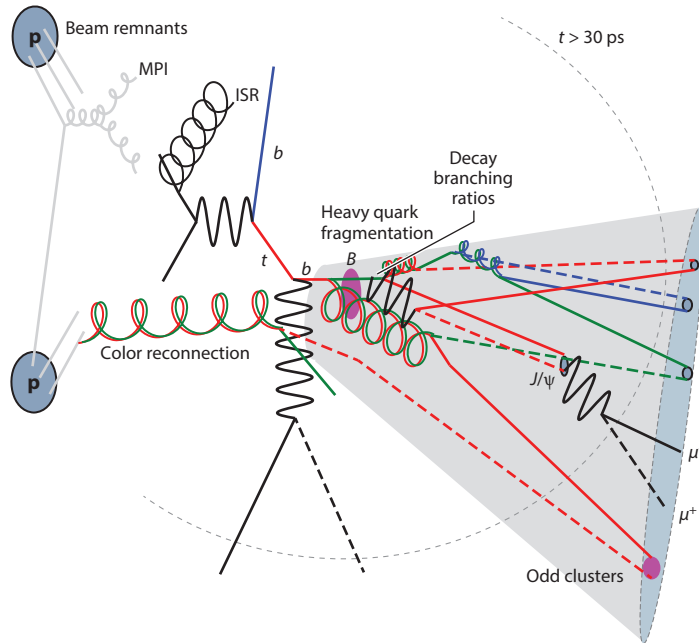


**Figure 1**

The main aspects modeled by a parton shower generator in a single top quark event. For a selected subset of partons, the QCD color flow is represented to illustrate the fragmentation and hadronization procedure that leads to a colorless final state. The typical time scale at which the generated particles are considered stable and impinging on the detector is represented by the gray dashed arc. Abbreviations: ISR, initial-state radiation; MPI, multiparton interaction; QCD, quantum chromodynamics.

The definition of the top quark mass in MC simulation and its mapping to a renormalization scheme is one of the properties subject to an intrinsic uncertainty from the definition of the top quark. Different PS algorithms use different evolution variables, and therefore one would expect them to alter the interpretation of the MC mass parameters. Several examples, using different observables, can be found in Reference 19. A recent review (20) points out that the uncertainty in identifying the MC mass with the pole mass is  $\mathcal{O}(500 \text{ MeV})$ . This is comparable to the experimental uncertainty in the direct measurements of the top quark mass. This example shows that although it is possible to correct measurements to a parton-level definition of the top quarks, such an operation implies an additional set of assumptions with respect to the detector response and reconstruction efficiencies. It introduces a dependency on the choice of PS and on nonperturbative QCD models. Thus, a parton-level definition is typically more sensitive to theory uncertainties than a particle-level one.

Whether the target is a particle-level or a parton-level top quark, experimental measurements need to be corrected and extrapolated, usually by means of a Poisson regression model (unfolding) (21). This operation has the disadvantage of correlating the individual measurements in each bin of the distributions and often dilutes the statistical significance. Nevertheless, such correction and extrapolation are most of the time unavoidable and may be mitigated by a careful choice of bins of the so-called migration matrix, which relates the reconstructed observable to the target one (22, 23).

## 2.2. Modeling Limitations or Discoveries?

The use of MC simulations at the LHC is crucial: Not only are they employed in the optimization and calibration of the measurements and searches, but they also are valuable for the interpretation of the parameters of interest. For top quark physics, the state-of-the-art matrix element (ME) generators typically have a next-to-leading-order (NLO) accuracy and involve a matching procedure to a PS generator, which takes over the evolution from parton-level objects to final-state particles through showering and hadronization. The PS generators also complete the description of the evolution of the proton remnants, additional partonic interactions, and color reconnection effects [i.e., the so-called underlying event (UE)]. **Figure 1** illustrates different aspects of this description, highlighting the ambiguity arising from color reconnection and the interference of radiation in production and decay. These effects are modeled phenomenologically and may obscure the direct interpretation of an event—for instance, when deciding whether a radiated parton should be considered part of the top quark decay products or not (24–26). Some of the aspects illustrated in **Figure 1** are also often the source of discrepancies between data and simulations.

MC simulations pose several challenges: from tuning the UE parameters, to the optimization of the matching algorithm between the ME and the PS generator, to the matching prescription necessary to avoid double-counting of phase space in the ME. The challenge of achieving accuracy and precision for physics can be partially addressed with ancillary measurements—for instance, by directly measuring top quark kinematics such as top quark  $p_T$  and jet activity (27–30), inspecting how well jets and their substructure are modeled (31–33), measuring the fragmentation function of heavy quarks (34, 35), or examining the surrounding UE (36). Provided that the phase space of such studies is largely decoupled from that used for the measurements or searches with top quarks, these are valid ways to improve shortcomings of the MC based on real data and adjust the values of phenomenological parameters and their range of uncertainty.

In addition to these physics-related issues, with high-integrated-luminosity data sets and accuracy, MC generation also poses several computing challenges implied by the several matching steps; these are described in detail in Reference 37.

## 2.3. Pushing the Detector Frontier

Top quark physics offers several opportunities to advance the detection and reconstruction frontiers: from developing new algorithms for reconstruction and background separation to improving the calibrations and online trigger selections. The variety of final states and the abundance of top quark events make this physics a perfect playground for such developments at the LHC and future colliders. The decay products of the top quark include heavy-flavored jets initiated by bottom quarks and either leptons from  $W \rightarrow \ell\nu$  or jets from  $W \rightarrow q\bar{q}'$  decays. Near-rest top quarks yield  $b$  jets with moderate energy,  $E_b \sim \mathcal{O}[(m_t^2 - m_W^2)/2m_t]$ , and fermions (leptons or light jets) from the  $W$  decays with a softer energy spectrum,  $E_f \sim \mathcal{O}(m_W/2)$ .

Charged lepton candidates are typically selected within an experiment's inner-tracking coverage—that is, in the central pseudorapidity region  $|\eta| = |-\ln \tan(\theta/2)| < 2.5$  ( $\theta$  denotes the polar angle) and with transverse momentum  $p_T > 20\text{--}30$  GeV. This ensures best efficiency, reduced momentum uncertainty, and the most precise association with a primary vertex. Quarkonia and  $Z$  boson events can be easily selected from the invariant mass of the two outgoing charged leptons and are typically used to both calibrate the momentum scale and measure lepton efficiencies. The latter attain uncertainties at the level of  $\lesssim 1\%$ .

Jets are usually reconstructed using the anti- $k_T$  algorithm with a parameter  $R = 0.4$  (38, 39). UE and pileup subtraction techniques, typically based on energy density and thresholds, are used to reduce the event-by-event fluctuations on the jet energy. The ATLAS and CMS experiments

follow similar calibration procedures, which involve mimicking the same operation in data and in MC simulation and applying a response scale factor. In data, additional response residuals are derived using events with a  $Z$  boson or photon and a recoiling jet, or multijet events that can be balanced in the transverse plane. The final uncertainty ends up being dominated by the so-called flavor uncertainty, owing to the difference in responses of the parton flavor initiating the jets that are used in the calibration samples (40, 41). The flavor response differences are estimated based on the comparison of the predictions from different PS generators [PYTHIA (42) and HERWIG (43)]. Such a source of uncertainty is hardly resolved with data, although with very high statistics one can use  $Z+b$  or  $\gamma+b$  (44, 45). Assuming the  $W$  boson mass, experiments are also able to use top quark–antitop quark ( $t\bar{t}$ ) events to calibrate the jet energy scale and resolution of light quarks using the resonant  $W \rightarrow qq'$  decay (46, 47). The relative  $b$ -to-light-jet energy scale can also be measured in situ using the  $t\bar{t}$  decay kinematics by taking a ratio of jet  $p_T$  sums:  $R_{bq} = [p_T(b) + p_T(\bar{b})]/[p_T(q) + p_T(\bar{q})]$ , a quantity that is accurately described in simulation and has reduced sensitivity to  $m_t$  (48). Experiments were able to achieve jet energy scale uncertainties of approximately 1–3% depending on the jet  $p_T$  and  $\eta$ . For  $p_T < 30$  GeV, pileup significantly degrades the jet energy scale uncertainty, while above 1 TeV, flavor uncertainties become subdominant and the experimental determination of the absolute scale is more relevant. With higher statistics, boosted top quark jets eventually may be used as a reference to improve on this uncertainty. The identification of heavy-flavored  $b$  jets benefits from optimal reconstruction of the impact parameter of the tracks and of displaced secondary vertices within the inner tracking systems. Such quantities are typically used to train multivariate algorithms (MVAs) used to discriminate  $b$  jets from jets initiated by lighter quarks or gluons. With the advent of machine learning (ML) techniques, the internal relation of all the reconstructed quantities of the jet constituents (kinematics, impact parameters, etc.) can be explored with finer granularity, thus significantly improving the efficiency in identifying heavy-flavored jets while substantially decreasing the misidentification of light-flavored jets. The calibration of all these algorithms can be done in  $b\bar{b}$ -enriched samples or in situ with  $t\bar{t}$  quark events (49–51).

In the high- $p_T$  regime the decay products become collimated and the jet gains a “hard scale” internal structure, which is distinct from the one generated by angularly ordered QCD emissions. As a rule of thumb, to identify the phase-space region where the boosted regime becomes relevant, one can use the distance in the rapidity–azimuth space of the decay products of a two-body decay given by  $\Delta R = \sqrt{\Delta\eta^2 + \Delta\phi^2} = 2m/p_T$ . For  $p_T(W) > 160$  GeV or  $p_T(t) > 345$  GeV, the  $W$  boson or top quark decay products typically will be separated by  $\Delta R \leq 1$  and can be reconstructed more efficiently using a larger cone jet. Recent developments have been made to bridge the resolved and boosted kinematic regimes to minimize losses in efficiency. An example is the use of a staggered approach where large- $R$  jets (e.g., 0.8) are initially used to find boosted top quarks, and in cases of failure, the fallback is standard resolved reconstruction (29). Alternatively, and motivated by theoretical partitioning based on  $N$ -jettiness (52), an exclusive cone jet algorithm such as X Cone (53) can bridge the two regimes while maintaining adequate efficiency. The advantage of such an algorithm is that it returns a fixed number of jets corresponding to the decay products of a top quark while it also functions as a grooming algorithm of the larger jet, significantly improving the resolution with respect to other classical algorithms used to reconstruct boosted resonances. Recently, this method has been successfully employed to measure the top quark mass from the X Cone jet mass (47, 54).

Another relevant quantity is the missing transverse energy ( $E_T^{\text{miss}}$ ), which is reconstructed by balancing all the particle candidates reconstructed in the event in the transverse plane. It is often used as input to resolve the neutrino kinematics. This quantity is perhaps the most sensitive to the overall calibration, pileup mitigation, and reconstruction strategies employed in the detector.

Particle flow (PF) algorithms are particularly suited for optimal  $E_T^{\text{miss}}$  resolution and in general for the global reconstruction of top quark events (55, 56). The contribution from the PF candidates for such an estimator can be weighted, taking into account the probability of pileup contamination, to improve the resolution (57).

Apart from the reconstruction challenges posed by top quark physics briefly illustrated above, there is also a major trigger challenge. With higher collision pileup and integrated luminosity, the natural tendency of the experiments is to raise the thresholds, cutting away a relevant phase space of top quark physics. To avoid this, part of the solution is to increase the granularity in the trigger of the experiments such that the online algorithms are closer to the ones used offline. This is becoming possible via the use of FPGA to perform fast and finer-granularity correlations between the different subdetectors. At a higher level, where processor farms are used, the deployment of heterogeneous computing architectures is also expected to help the experiments cope with the anticipated increases in trigger rates (58–60). Future upgraded detectors for Phase 2 of the LHC will also include precision timing layers with a resolution  $\mathcal{O}(30\text{ ps})$  for minimum ionizing particle-like deposits, improved tracking devices, and finer-granularity calorimeters that will provide the necessary experimental handles to improve the disambiguation of the hard processes from the surrounding pileup environment (61, 62). Such developments will be crucial to ensure that top quark physics can be performed in the LHC phase that will deliver up to  $3\text{ ab}^{-1}$  of data ( $\sim 10$  times larger than produced in the current phase).

### 3. TOP QUARK PRODUCTION AT THE LHC

At the LHC, the top quark is predominantly produced in  $t\bar{t}$  pairs but also singly, as illustrated by the most relevant leading-order (LO) diagrams in **Figure 2**. The main characteristics and merits of studying these production modes separately are summarized in the subsections below.

#### 3.1. Top Quark Pair Production

At the center-of-mass energy of the LHC, gluons dominate the parton distribution functions (PDFs) of the colliding protons. Therefore,  $t\bar{t}$  production is the dominant top quark production

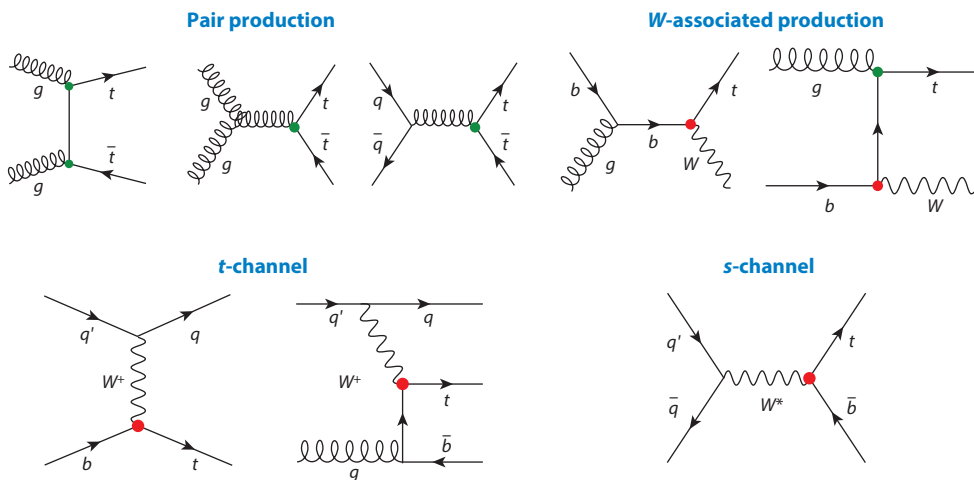


**Figure 2**

Representative diagrams for strong production of top quark–antiquark pairs, electroweak single top quark production in the  $t$ - and  $s$ -channels, and  $W$  boson–associated production. The top quark couplings to gluons are indicated by green circles; couplings to  $W$  bosons are indicated by red circles.

mode in **Figure 2** since most  $t\bar{t}$  pairs are produced through gluon fusion,  $gg \rightarrow t\bar{t}$  (80–90%), with a modest estimated fraction of 20–30% being color-singlet states. Although it is expected that near-threshold production of  $t\bar{t}$  is sensitive to small bound-state effects (63, 64), these are expected to be unstable, in contrast to the lighter quarkonia resonances. This instability is mostly driven by the short lifetime of the top quark (see Section 2.1).

The on-shell production of  $t\bar{t}$  pairs requires a relatively high energy transfer ( $Q \geq 2m_t$ ), and thus the relative momentum fraction of the incoming partons ( $x$ ) is typically high:  $x \gtrsim 0.03$  at  $\sqrt{s} = 13$  TeV and  $x \gtrsim 0.07$  at  $\sqrt{s} = 5.02$  TeV. An accurate theory prediction of the  $t\bar{t}$  cross section requires, in addition to the calculations of virtual and real contributions, the resummation of soft-gluon terms, enhanced by the large mass, as  $\alpha_s^n \log^k(m/Q)$  terms become sizable. The next-to-next-to-leading order (NNLO), including next-to-next-to-leading log (NNLL) soft-gluon resummation, predicts the total cross section to be  $\sigma(t\bar{t}) = 832_{-29}^{+19}$  (scale)  $_{-35}^{+35}$  (PDF) (65, 66) at  $\sqrt{s} = 13$  TeV, with the first uncertainty from the QCD scale and the second from the PDF.

Several inclusive and fiducial  $t\bar{t}$  production cross sections have been measured covering different  $\sqrt{s}$  values, colliding beams, and final states. Measurements have covered proton–proton collisions at 5.02 TeV (67, 68), 7 and 8 TeV (69), and 13 TeV (70, 71) and typically have been more precise for final states with an electron and a muon. Special measurements in the forward ( $2.0 < \eta < 4.7$ ) region (72, 73), in proton–nucleus collisions (74), and in nucleus–nucleus collisions (75) have also been made. In general, the measurements agree with the theory predictions (see **Figure 5** in Section 3.6 below). When made with the high-integrated-luminosity data sets, the measurements attain uncertainties of  $\mathcal{O}(2\text{--}3\%)$ , which are dominated by uncertainties in integrated luminosity and the trigger- and lepton-selection efficiencies.

The dependency of the cross section on  $\alpha_s$  and on  $m_t$  can be used to extract these two fundamental parameters of the SM. The extraction is theoretically safe because the cross section calculation uses an  $m_t$  defined in a fixed renormalization scheme, unlike the  $m_t$  parameter used in a PS program (see Section 2.2). There is, however, a residual uncertainty from contributions from nonperturbative corrections, which arises partially from the PDFs and from the mechanism used to dress the QCD color charge carried by the top or antitop quark. These effects occur at a scale  $\sim \Lambda_{\text{QCD}}$ , and although for most cross section measurements  $Q \gg \Lambda_{\text{QCD}}$  (and  $\sigma > \sigma_{\text{NP}}$ ), they limit the precision of the extracted SM parameters (20). In the most recent combination of LHC Run 1 (69), the pole mass is measured with a relative uncertainty of 1.2% ( $m_t^{\text{pole}} = 173.4_{-2.0}^{+1.8}$  GeV), and  $\alpha_s(m_Z)$  is measured with a 1.8% relative uncertainty:  $\alpha_s(m_Z) = 0.1170_{-0.0018}^{+0.0021}$  for the chosen PDF reference. The latter result is found to be in good agreement with other determinations of  $\alpha_s(m_Z)$  and to rival them in precision. The somewhat limiting factors of these measurements (choice of renormalization and factorization scales and PDFs) can be partially overcome with differential cross section measurements. A promising avenue has been explored in the triple differential measurement of the production cross section as a function of  $m(t\bar{t})$ ,  $y(t\bar{t})$ , and additional jet multiplicity (76). This approach allows for the partial decorrelation of  $\alpha_s$ ,  $m_t$ , and PDF and a simultaneous fit of the three parameters with competing uncertainties. Other improvements in the uncertainty of  $m_t$  were obtained using the boosted top quark jet mass line shape in the high- $p_T$  regime (47) and the invariant mass of the system formed by a  $t\bar{t}$  pair and an additional jet (77, 78). Future analyses, using the full LHC data sets, may reach  $<1\%$  relative uncertainty in these fundamental parameters.

Differential  $t\bar{t}$  production measurements have been performed in different final states as a function of several kinematic variables ( $d\sigma/dX$ ) and employing different reconstruction algorithms. The main challenges are related to the purity and stability of the observables. Purity is the estimator for the fraction of reconstructed events that also correspond to generated events in a given interval, while stability estimates the fraction of generated events that are reconstructed in the

corresponding interval. They are linked to the so-called confusion matrix of a reconstruction algorithm and quantify the effectiveness of the unfolding procedure. Variables reconstructed with high resolution (e.g., from charged leptons) or employing optimized reconstruction algorithms are preferable to avoid overly coarse measurements of  $d\sigma/dX$ . The inversion is made to a fiducial phase space and to a particle- or parton-level definition of the top quark. A direct comparison with fixed-order calculations requires the correction of “parton level” used in the computation of an ME. This nontrivial extrapolation involves adjusting for the nonperturbative effects (see Section 2.1) inherent in the modeling. Different observables are used to probe different aspects with four simple categories:  $t\bar{t}$ , individual top quark, final state, and global event variables.

The  $t\bar{t}$  system is sensitive to the proton PDF through its rapidity  $y(t\bar{t}) \sim 1/2 \log(x'/x)$ . With respect to a dijet system,  $t\bar{t}$  events have the advantage of being sensitive to high  $x$  and high  $Q^2$  already at threshold. The  $t\bar{t}$  transverse momentum is mostly sensitive to initial-state radiation (ISR) and is thus an interesting test of perturbative QCD (pQCD). The invariant mass of the  $t\bar{t}$  system,  $m_{t\bar{t}}$ , is more intricate: It is sensitive to threshold effects [ $m_t$ ,  $t$ - $H$  Yukawa coupling ( $y_t$ ), bound-state effects], the running of  $\alpha_s$ , and BSM contributions. Quantum interference effects from BSM contributions may add to the complexity of analyzing  $m_{t\bar{t}}$ . The  $m_{t\bar{t}}$  spectrum is affected by uncertainties in the jet energy scale and resolution and by statistics at low and high  $m_{t\bar{t}}$ , which often limit the experimental reach. Recently, this observable has been used to test the running of the top quark mass, as given by the renormalization group equation (79). Experimentally, this analysis makes use of a multidimensional fit to  $m_{t\bar{t}}$  but also to the jet  $p_T$  and  $m_{lb}$ , depending on the  $b$  jet multiplicity and jet multiplicity. This technique has the advantage of constraining in situ some experimental uncertainties (such as  $b$  tagging and jet energy scale), increasing the sensitivity to the parameter under investigation. It is expected that in the future, such techniques can improve the precision of indirect measurements from  $m_{t\bar{t}}$ . Particularly interesting is the indirect extraction of the Yukawa coupling from the  $m_{t\bar{t}}$  spectrum. Using the full Run 2 data and the dilepton final state (80), the CMS experiment obtained a higher bound of  $y_t < 1.54 y_t^{\text{SM}}$  at the 95% confidence level (CL). Although this measurement has a larger uncertainty compared with direct measurement of  $y_t$  through Higgs cross sections, including  $t\bar{t}H$  production (81, 82), it relies less on the assumed decay branching ratios (BRs) of the Higgs boson.

Measurements of the individual top quark kinematics provide stringent tests of the theory at different scales as they are sensitive to pQCD, resummation effects, and EW corrections. A particular case is the top quark  $p_T$ . Recent developments in jet algorithms and event reconstruction techniques have enabled a coherent measurement in the full kinematic range (boosted and nonboosted regimes)—up to 1.6 TeV (28, 29, 83), with fair agreement with NNLO QCD—whereas the typical NLO QCD generators tend to predict a significantly harder  $p_T$  spectrum, overestimating the cross section at high  $p_T$ .

Recent measurements of the final-state kinematics (27, 84, 85) and properties (e.g., fragmentation functions, color flow, substructure) (32–34) are sensitive to higher-order corrections and can be used to improve the modeling of the MC generators, aiming for a better baseline calibration for the extraction of fundamental parameters. Particularly noteworthy are measurements in the dilepton final state as they have reduced QCD color flow, simplifying the calculation of higher-order terms. Still, a correct description must formally include off-shell and non-double-resonant effects in top quark production (86–88) as well as resonance mass effects in production and decay (89, 90) using a narrow-width approximation (91). Theory advances have been made on these fronts with different accuracy and also in interfacing NNLO calculations with PS (92, 93). Although leptons are produced later in the decay chain, they still preserve sensitivity to several properties of the top quark production and decay. Because their spectra are reconstructed with very good resolution, they are less prone to modeling uncertainties when unfolded and serve as good comparisons with

state-of-the-art calculations. Although at this point there is no direct comparison with a theory model containing all the corrections mentioned above, measurements such as those described in References 31, 70, 85, 94, and 95 show that no single NLO + PS generator can satisfactorily describe the full phase space or all variables. There are significant improvements when higher-accuracy predictions in the fiducial phase space are included in the  $p_T$  of the final-state objects or in variables correlating two final-state objects such as  $m(\ell b)$  and  $\Delta\phi(\ell\ell')$ . The latter are discussed in more detail below in the context of spin correlations. Measurements of the fragmentation functions and jet substructure also advance the field and are particularly important to more accurately interpret the so-called direct top quark mass measurements using either jets or  $B$  hadrons, to stress the universality assumption on  $b$  fragmentation, and to improve the general understanding of the algorithms used to identify  $b$  jets. On this front, the data show fair agreement with the Large Electron–Positron Collider (LEP)-based tuning of  $b$  fragmentation (34), although some substructure-related variables cannot be fully described by the same PS and tuning for all the jet flavors in a  $t\bar{t}$  event (33). Substructure-related variables—in particular, variables such as the groomed momentum fraction ( $z_g$ ) and the angle between groomed jets ( $\Delta R_g$ )—show sensitivity to  $\alpha_S$  and can be used to extract it. When the highest-accuracy prediction using leading log with rescaling to account for next-to-leading corrections to soft-gluon emissions (96) is used,  $\alpha_S$  is measured with a 13% relative uncertainty. Although comparably worse than the measurements from the inclusive cross section, this result significantly constrains the uncertainty in final-state radiation (FSR) in the PS model. With higher-accuracy calculations and updated measurements, this approach is also expected to significantly improve the precision of future top quark measurements.

Finally, measurements of global event variables such as those reported in References 36, 97, and 98, and measurements related to the production in association with jets, are crucial since they allow for an improved description of the  $t\bar{t}$  system as a background for rarer processes such as  $t\bar{t}H$  and  $t\bar{t}\bar{t}$  production. The associated production with heavy-flavored jets is discussed below.

It must be noted that the categorization above is somewhat artificial since, as mentioned in Section 2, several effects become correlated in the reconstruction of each top quark and the  $t\bar{t}$  system or are still present in the final-state particles. Thus, in principle, only a global fit of all relevant variables is able to correctly capture the interdependencies and sensitivity to fundamental parameters and phenomenological modeling handles used in PS simulations.

Different measurements provide additional insight when backed by specific physics models. An example is the measurement of the spin-density matrix of the  $t\bar{t}$  system. When produced in pairs, the top and antitop quarks effectively form a natural two-qubit system (99), with their spins strongly correlated, despite the small individual polarization predicted by mixed QCD-EW contributions (100). Measurement of these correlations provides a test of quantum entanglement and, eventually, of violation of Bell’s inequalities (99, 101). The MEs that describe  $t\bar{t}$  production are directly proportional to the production density matrix ( $R$ ) that describes the transition amplitude from the initial four-momenta of the partons to the four-momenta and spin four-vector of the  $t\bar{t}$  system and that is typically decomposed as

$$R^l = \frac{(4\pi\alpha_S)^2}{\kappa_l} \left[ \tilde{A}^l \mathbb{I} \otimes \mathbb{I} + \tilde{B}_i^{l+} \mathbb{I} \otimes \sigma^i + \tilde{B}_i^{l-} \mathbb{I} \otimes \sigma^i + \tilde{C}_{ij}^l \sigma^i \otimes \sigma^j \right], \quad 3.$$

where the index  $l$  distinguishes the nature of the incoming partons,  $\kappa_l$  is a QCD-color-related factor,  $\tilde{A}$  is constant and reflects a spin-averaged production at the parton level of  $d\sigma/d\Omega d\hat{s} \propto \tilde{A}/\hat{s}^2$ ,  $\tilde{B}^\pm$  are three-vectors describing the top and antitop quark degrees of polarization along each axis,  $\tilde{C}$  is a  $3 \times 3$  matrix describing the spin correlation of the pair along each pair of axes, and  $\sigma^i$  are the Pauli matrices. This formulation can be used to express the cross section as a function of the top quark scattering angle and can thus be related to experimental observables. The customary

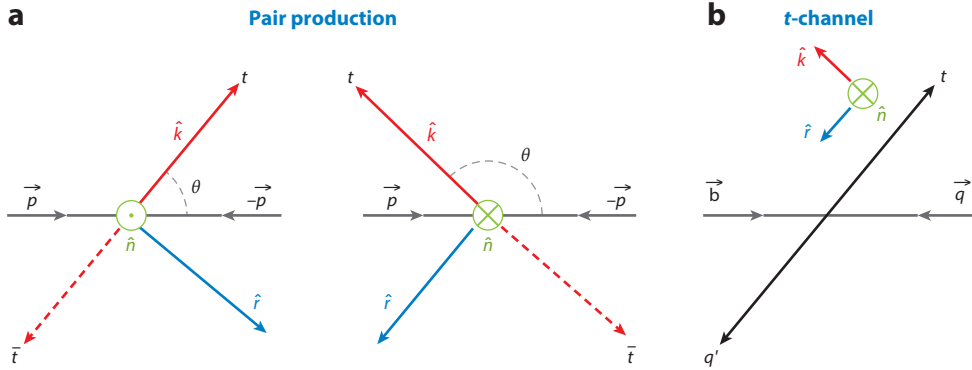


**Figure 3**

Right-handed orthonormal basis used to analyze top quark production in the zero-momentum frame. The diagrams in panel *a* are used to analyze the  $t\bar{t}$  system spin. Two representative scattering angles are shown where the signs of  $\hat{r}$  and  $\hat{n}$  are flipped, taking into account the sign of the scattering angle and hence defining a forward direction in the represented events. The incoming and outgoing parton ( $t\bar{t}$ ) directions are represented in addition to the basis vectors. The diagram in panel *b* represents the natural definition for single top quark production with the helicity axis pointing in the direction of the spectator quark.

choice for defining the components of the  $R$  matrix uses a right-handed orthonormal basis where the top quark direction in the  $t\bar{t}$  rest frame defines a helicity axis ( $\hat{k}$ ), the top and antitop quark production plane is used to define a perpendicular axis ( $\hat{n}$ ), and the third axis is orthogonal to the first two ( $\hat{r}$ ). The Bose symmetry of the  $gg$  initial state implies that  $R^{gg}(-\vec{p}, \vec{k}) = R^{gg}(\vec{p}, \vec{k})$ , which is nonvanishing only if  $\hat{n}$  and  $\hat{r}$  are defined in such a way that they take into account the sign of the scattering angle, as sketched in **Figure 3a**. In this way, a forward direction can be defined for each event.

The spin effects inherited by the decay products result in an angular distribution correlated with the spin axis through

$$\frac{1}{\Gamma_t} \frac{d\Gamma_t}{d\cos\vartheta} = \frac{1}{2} (1 + \kappa P \cos\vartheta), \quad 4.$$

where  $\vartheta$  is the angle between the direction of flight of the decay product and a properly chosen spin quantization axis,  $P$  is the top quark's degree of polarization along this axis, and  $\kappa$  is the so-called spin-analyzing power of the decay product. The spin-analyzing power is maximal for charged leptons ( $\approx 1$ ) and is approximately  $-0.39$  for the bottom quarks (102). This property can be used to simplify the determination of the elements of Equation 3 from the angular distributions of leptons. The ATLAS and CMS experiments have measured both the spin-density MEs (103, 104) and the top quark polarization (105, 106) using the angular distributions of the leptons. In general, the coefficients measured exclude a fully spin-uncorrelated scenario and agree with NLO predictions [for the 22 observables,  $\chi^2/\text{dof} \approx 89/100$  (104)]. Among all the observables inspected,  $\Delta\phi(\ell, \ell')$ —the azimuthal angle between the two leptons—is particularly interesting given its high experimental precision and smaller extrapolation uncertainty (it does not require a top quark reconstruction). Comparison with NLO + PS predictions yields poor agreement, which improves at NNLO QCD (89), as depicted in **Figure 4**. This sensitivity reflects the delicate balance needed when searching or excluding BSM contributions with top quarks. In the specific case of the  $\Delta\phi(\ell, \ell')$  observable, the spectrum could be distorted if the polarization of the top quarks is altered—for instance, from anomalous chromomagnetic moments or if the top quark is produced after the decay of a supersymmetric top quark partner (the stop,  $\tilde{t}$ ). The current level of agreement

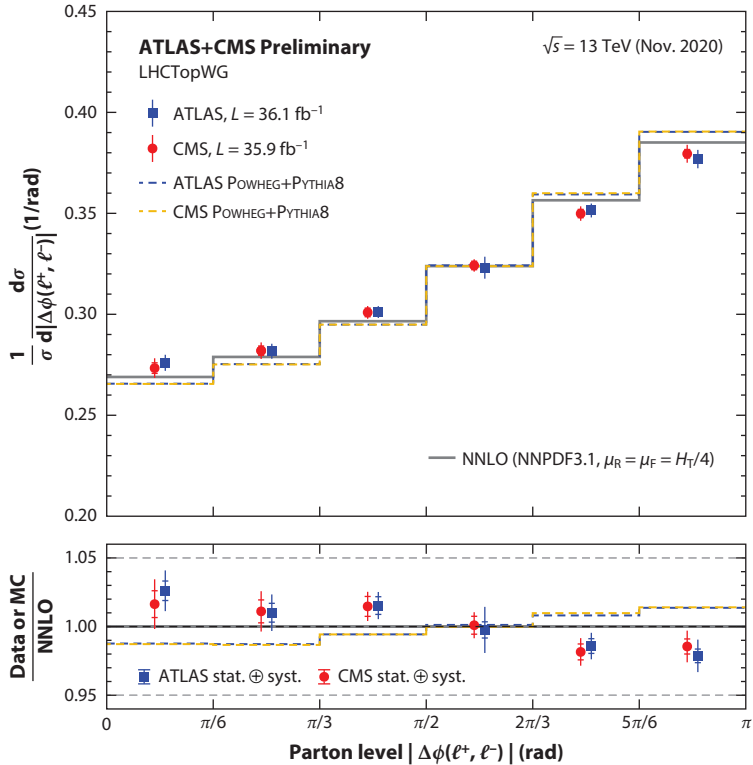


**Figure 4**

ATLAS (105) and CMS (104) data compared with NLO QCD + PS simulations as well as NNLO calculations (89) in perturbative QCD. The ATLAS and CMS data are corrected to the parton level. Abbreviations: LHC TopWG, LHC Top Physics Working Group; MC, Monte Carlo; NLO, next-to-leading order; NNLO, next-to-next-to-leading order; PS, parton shower; QCD, quantum chromodynamics. Figure adapted from Reference 107 (CC BY 4.0).

excludes  $170 < m_{\bar{t}} < 230$  GeV at 95% CL (105). However, these interpretations are based on an NLO estimation that, as illustrated above, may be insufficient. With increased statistics it will be interesting to extend these measurements to different fiducial regions since they have the potential to uncover BSM contributions in  $t\bar{t}$  production. Measurement in different  $m_{\bar{t}}$  ranges has been pioneered in Reference 105.

### 3.2. Single Top Quark Production

Besides being produced in pairs, top quarks can be produced singly through their EW couplings (Figure 2). In single top quark events, the structure of the  $tWq$  vertex is isolated from the additional QCD couplings that are present in strong  $t\bar{t}$  production. In the particular case of single top quark production in the  $t$ - and  $s$ -channels, the top quark is practically 100% polarized given that it results from a parity-violating process. A notable feature is that the  $tWq$  vertices contribute twice (at production and at decay), increasing the sensitivity of these channels to squared terms of  $V_{tb}$ .

The  $s$ -channel has been established at the LHC by the ATLAS Collaboration using  $\sqrt{s} = 8$  TeV (108) and 13 TeV (109) with a significance of  $3.2\sigma$  and  $3.3\sigma$ , respectively. The process has also been searched in the CMS experiment (110). The main challenge in isolating this process

lies in discriminating the signal against the overwhelming  $t\bar{t}$  and  $W$  + heavy flavor background. So far, this has been achieved by using an ME-based technique (MEM), in which a per-event probability of compatibility with the signal hypothesis is assigned. In the MEM, the probability density is computed from the differential cross section, and a transfer function is used to translate from the parton level to the reconstructed objects while taking into account measured resolutions and efficiencies of the objects used in the analysis. The output of the MEM discriminator is converted to a probability measurement in a signal-plus-background ensemble hypothesis,  $P(S|X)$ , using Bayes's theorem. The distribution of  $P(S|X)$  is then validated in signal-depleted regions and is fitted in the signal region where a single charged lepton, two  $b$  jets, and missing transverse energy are required. The likelihood fit of  $P(S|X)$  yields the final normalizations of the different processes in the signal region and reduces some uncertainties, most notably those related to  $t\bar{t}$  modeling, in situ. At  $\sqrt{s} = 13$  TeV, the expected cross section computed at NLO (111, 112),  $\sigma_{s\text{-ch}}^{\text{theor}} = 10.32_{-0.24}^{+0.29}$  (scale) $_{-0.26}^{+0.27}$  (PDF +  $\alpha_s$ ) pb, is in good agreement with the observed value,  $\sigma_{s\text{-ch}}^{\text{obs}} = 8.2_{-2.9}^{+3.5}$  pb.

In the  $t$ -channel, the top quark is produced in association with a forward jet, which provides a distinctive signature with a rapidity gap in between, formed after the color-singlet exchange. This process has been observed in the ATLAS and CMS experiments at  $\sqrt{s} = 7$  and 8 TeV (113). At  $\sqrt{s} = 13$  TeV, the  $t$ -channel NLO cross section is expected to be  $\sigma_{t\text{-ch},t} = 136.0_{-2.9}^{+4.1}$  (scale) $_{-3.5}^{+3.5}$  (PDF +  $\alpha_s$ ) pb for the top quark and  $\sigma_{t\text{-ch},\bar{t}} = 81.0_{-1.6}^{+2.5}$  (scale) $_{-3.2}^{+3.2}$  (PDF +  $\alpha_s$ ) pb for the antitop quark (111, 112). The charge-asymmetric production provides an interesting experimental test of the quark–antiquark PDFs of the protons. These expectations, as well as those at lower energy, are in good agreement with experimental results (113–115). More recent, higher-order, NNLO calculations (116, 117) require handling of the interference with the  $s$ -channel that is expected at higher orders in the five-flavor scheme (5FS). Although the NNLO predictions have similar accuracy, their relative uncertainty is reduced by approximately 70% with respect to NLO. With the advent of NNLO + PS, this improvement is expected to have a significant impact in future measurements given that the limiting systematic uncertainties are currently related to the modeling of the signal—namely, PS-related uncertainties. The  $t$ -channel differential cross sections have also been measured at different  $\sqrt{s}$  values with increasing precision (118, 119). Fair agreement is found overall with the NLO predictions favoring the so-called four-flavor scheme (4FS) computations where the bottom quark is treated as a massive object at the level of short-distance cross section and does not appear in the initial state. Not surprisingly, the distribution of the top quark  $p_T$  is particularly sensitive to the comparisons with the 4FS or 5FS predictions (119). Given the  $V - A$  form of the  $tWb$  vertex, in the  $t$ -channel the top quark's spin is aligned with the direction of the down-type quarks. The production is dominated by diagrams where the down-type quark is a spectator quark and has a smaller contribution from diagrams where the down-type antiquark is incoming. Thus, the degree of polarization (see Equation 4) depends slightly on the mixture of the two production processes. As it is experimentally challenging (and not infrared-safe) to identify the jet with the quark electric charge, the convention is to choose the direction of the spectator quark in the rest frame as the helicity axis, as depicted in **Figure 3b**. As noted for the  $t\bar{t}$  case (Equation 4), the charged lepton has maximal spin-analyzing power, with  $\kappa_{\ell^\pm} = \pm 0.998$  at NLO and polarizations  $P_t = 0.91$  and  $P_{\bar{t}} = -0.86$ , also at NLO (102, 120). The measured  $\cos\theta^*$  distribution is reported in References 119, 121, and 122 and is in good agreement with the SM expectations. In an analogous manner to that done for the  $t\bar{t}$  case, the spin-density MEs for the different  $W$  boson helicities can be measured, as pioneered in Reference 121. Overall, these measurements are found to be in agreement with the SM predictions and are used to limit anomalous couplings (121, 123).

The associated  $tW$  production is of particular interest because it mixes QCD and EW couplings and can be separated from  $t\bar{t}$  production only at lower orders in perturbation theory. At  $\sqrt{s} = 13$  TeV, the NLO + NNLL  $tW$  cross section is  $\sigma_{t\bar{t}} = 71.7 \pm 1.8$  (scale)  $\pm 3.4$  (PDF +  $\alpha_s$ ) pb (124, 125). However, at NLO,  $tW$  is part of a larger set of processes that includes double-resonant ( $t\bar{t}$ ) and single-resonant ( $tW$ ) top quark production and quantum interference between the two (126–128). The separation at NLO of these contributions is typically achieved either by removing the double-resonant diagrams (the DR approach) or by modifying the differential cross section with a gauge-invariant subtraction term (the DS approach) (126, 129). Based on this paradigm, the single-resonant production has been measured at different  $\sqrt{s}$  values and found to be in agreement with the theory predictions (113, 130, 131). The discrimination against the double-resonant  $t\bar{t}$  background is typically made using MVA discriminators where the balance of the final-state objects in the transverse plane, the additional jet multiplicity, and the  $p_T$  of the objects rank high as discriminating variables. The results show good agreement with NLO QCD predictions (relative uncertainty  $\approx 10\%$ ). The main uncertainty is related to the modeling of the dominant  $t\bar{t}$  background and the  $tW$  signal, while experimentally the jet energy scale and resolution-related uncertainties also contribute significantly. Although the precision is lower because of its lower purity, this process has also been observed in the lepton-plus-jets final state, which enables full reconstruction of the kinematics (132). First measurements of the production cross section as a function of different variables have been made with the higher-luminosity data sets at  $\sqrt{s} = 13$  TeV (95, 131, 133). Given the overall strategy chosen to discriminate signal from background based on MVA discriminators, the unfolding procedure needs to correct for possible biases introduced in the observables from the discriminator itself, in addition to the standard reconstruction and particle- to parton-level corrections. Likewise, in the  $t\bar{t}$  differential measurements, both the  $\Delta\phi(\ell^+, \ell^-)$  and the top quark  $p_T$  distributions are at odds ( $p$  value  $\ll 10\%$ ) with the NLO QCD predictions for different ME and PS generator settings. None of the variables are particularly sensitive to the DR or DS schemes mentioned above. A particularly interesting test is made in Reference 95 for the quantum interference between double-resonant and single-resonant diagrams inspecting the invariant mass of the lepton +  $b$  jet system. The variable  $m^{\text{minimax}}(\ell b) = \min\{\max[m(\ell_1 b_1), m(\ell_2 b_2)], \max[m(\ell_2 b_1), m(\ell_1 b_2)]\}$  is used for this purpose. Beyond the LO end point of this spectrum,  $m(\ell b) < \sqrt{m_t^2 - m_W^2}$ , and for close-by systems with low  $m(\ell, b) < 40$  GeV, this observable is sensitive to the DR or DS scheme. In particular, at high mass ( $> 160$  GeV), where off-shell and nonresonant productions are expected to be more relevant, the DR scheme tends to overestimate (and the DS scheme tends to underestimate) the observed data with  $p$  values  $\leq 57\%$  for alternative predictions. However, if the higher-order calculation of Reference 134 is used, including interference effects, the data show significantly better agreement with the SM prediction, reaching a  $p$  value of 95%. This result paves the way for future measurements of inclusive  $t\bar{t} + tW$  cross sections.

As a general summary, single top quark cross section measurements agree with theory predictions at NLO (see **Figure 5** in Section 3.6 below). Among all the single top quark channels, the  $t$ -channel is the golden channel thanks to its purity and high yield. The experimental precision attained is sufficient for the extraction of  $V_{tb}$ , as explained above. The inclusive single top quark cross section measurement yields a combination of  $V_{tb}$  and a form factor for the  $tWb$  interaction ( $f_{LV} = 1$  in the SM) through

$$|f_{LV}V_{tb}| = \sqrt{\frac{\sigma_{t\text{-ch}}^{\text{obs}}}{\sigma_{t\text{-ch}}^{\text{theor}}}}. \quad 5.$$

For other fundamental parameters of the theory, such as  $m_t$ , the sensitivity is poorer compared with  $t\bar{t}$ .

The Run 1 combination of all single top quark measurements attains a 4.4% relative uncertainty (113) using the NLO theory reference and has not been surpassed yet by inclusive 13-TeV measurements. This result can be improved with higher-accuracy predictions and also with dedicated differential measurements. A recent example can be found in Reference 135, which obtains  $|V_{tb}| = 0.988 \pm 0.024$  and  $|V_{td}|^2 + |V_{ts}|^2 = 0.06 \pm 0.06$  when SM-like constraints are released and a lower bound of  $|V_{tb}| > 0.970$  at 95% CL with SM-like assumptions. This is a promising result given that it relaxes SM-based assumptions in the measurement of  $R_b = B(t \rightarrow Wb) / \sum B(t \rightarrow Wq)$ , which yields the most precise constraint on  $V_{tb} > 0.975$  at 95% CL. The combination of  $R_b$  with  $\sigma_{t\bar{t}}$  is also used to measure  $\Gamma_t = 1.36 \pm 0.02$  (stat.) $_{-0.11}^{+0.14}$  (syst.) GeV (136).

### 3.3. Associated Production of Top Quarks and Bosons

The associated production of top quarks (single or in pair) and bosons ( $\gamma$ ,  $W$ ,  $Z$ ,  $H$ ) has a rich phenomenology and sensitivity to BSM physics. Because these are high-mass states that involve typically weaker couplings, the cross sections are small ( $\ll 1$  pb). Setting aside  $tHq$ , all processes in which a single boson is produced in association with top quarks have already been established experimentally, as illustrated in **Table 1**.<sup>1</sup> With high-integrated-luminosity data sets, some of these processes have reached good precision and can be measured differentially.

The associated production with a  $\gamma$  or  $Z$  boson proceeds through similar diagrams. There are, however, some subtleties in defining these processes. In the  $\gamma$  case, there is a nonnegligible probability of it being radiated from a final-state charged particle. Appropriate phase-space selections may reduce these contributions (experiments typically require photon isolation and minimum  $\Delta R$  separation from the objects). Moreover, final-state particles receive contributions from both  $tW\gamma$  and  $tWZ$ , which constitute irreducible backgrounds, of  $\mathcal{O}(6\%)$ , and are somewhat analogous to the  $t\bar{t}$  and  $tW$  case (see Section 3.1). In the  $Z$  case, the contribution of  $\gamma^* \rightarrow \ell\bar{\ell}$  is also relevant, even if largely suppressed by the requirement of the vicinity of  $m(\ell\bar{\ell})$  to the  $Z$  pole mass. The combined measurement of the  $Z$ - and  $\gamma$ -associated processes is expected to disambiguate the different EW dipole operators of the top quark (178). In addition, the interference between diagrams where the photon comes from ISR or from FSR yields an intrinsic asymmetry of the  $t\bar{t}$  system already at LO and increases the relative contribution of  $q\bar{q}$  production, providing handles that can be used to probe BSM scenarios (179). In single top quark-associated production, diagrams that include triple gauge coupling contributions from  $WW\gamma$  and  $WWZ$  are implicit and may provide additional handles for EW fits for these couplings. Overall, the measurements are found to be in agreement with the NLO predictions, both inclusive and differential. The  $t\gamma q$  process is observed with a somewhat higher [ $\mathcal{O}(33\%)$ ] cross section and an approximately 11% uncertainty. The relative uncertainty attained in  $t\bar{t}Z$  is approximately 10% and dominated by statistical and lepton-selection-efficiency-related uncertainties. In the  $t\bar{t}\gamma$  case, the uncertainty of the measurements (4–6%) is dominated by signal modeling. For the  $tZq$  and  $t\gamma q$  processes, the uncertainties (12–15% and 30%, respectively) are still dominated by the statistical component, followed by systematic uncertainties related to the background estimations, the jet energy scale, and lepton-selection efficiencies.

In  $t\bar{t}W$  LO, the boson is generated from  $q\bar{q}$  initial states, with the gluon splitting producing  $t\bar{t}$ . It is an ISR-initiated and charge-asymmetric process owing to the proton PDFs, with  $\sigma(t\bar{t}W^+) \approx 1.9 \cdot \sigma(t\bar{t}W^-)$ . Nevertheless, higher-order corrections open new channels, color flow, and flavor structures, which enhance the cross section with respect to the LO prediction. As summarized in **Table 1**, the vast majority of the  $t\bar{t}W$  measurements have used final states that comprise either

<sup>1</sup>The associated  $tW$  production is omitted in **Table 1** because it is discussed separately in Section 3.2.

**Table 1** Summary of final states covered experimentally in associated top quark–boson productions

Process	$\sigma$ or $\sigma_{\text{fid}}$ (fb)	$t\bar{t}$ decay	Boson decay	Channel	BR (%)	References for measurements
$t\bar{t}\gamma$	$495 \pm 99^a$	$(\ell^\pm \nu b) (q\bar{q}b)$	—	$1\ell$	34.4	137–141
	$63 \pm 9^a$	$(\ell^\pm \nu b) (\ell^\mp \nu b)$	—	$2\ell\text{OS}$	6.5	139, 142, 143
$t\gamma (+q)$	$81 \pm 4^b$	$(\ell^\pm \nu b)$	—	$1\ell$	25.6	144, 145
$t\bar{t}Z$	$840 \pm 100^c$	$(\ell^\pm \nu b) (q\bar{q}b)$	$q\bar{q}$	$1\ell$	24.1	146
		$(\ell^\pm \nu b) (\ell^\mp \nu b)$	$q\bar{q}$	$2\ell\text{OS}$	4.6	147, 148
		$(q\bar{q}b) (q\bar{q}b)$	$\ell^\pm \ell^\mp$		4.5	147, 149
		$(\ell^\pm \nu b) (q\bar{q}b)$	$\ell^\pm \ell^\mp$	$3\ell$	2.3	147–156
		$(\ell^\pm \nu b) (\ell^\mp \nu b)$	$\ell^\pm \ell^\mp$	$4\ell$	0.4	147–151, 153–156
$tZ (+q)$	$94 \pm 3.1^d$	$(\ell^\pm \nu b)$	$\ell^\pm \ell^\mp$	$3\ell$	1.7	156–160
$t\bar{t}W$	$592^{+155}_{-97}^e$	$(\ell^\pm \nu b) (q\bar{q}b)$	$\ell^\mp \nu$	$2\ell\text{OS}$	4.4	147
		$(\ell^\pm \nu b) (\ell^\mp \nu b)$	$q\bar{q}'$		4.4	147
		$(\ell^\pm \nu b) (q\bar{q}b)$	$\ell^\pm \nu$	$2\ell\text{SS}$	4.4	147–150, 152–154, 161
		$(\ell^\pm \nu b) (\ell^\mp \nu b)$	$\ell^\pm \nu$	$3\ell$	1.7	147–150, 161
$t\bar{t}H$	$507^{+35}_{-50}^f$	$(\ell^\pm \nu b) (q\bar{q}'b)$ $(\ell^\pm \nu b) (\ell^\mp \nu b)$	$b\bar{b}$	$1\ell$ or $2\ell\text{OS}$	23.8	162–166
		Inclusive	$\tau\tau, WW, ZZ$	Multileptons	30.4	163, 166–168
		Inclusive	$\gamma\gamma$	$\gamma\gamma+X$	0.2	163, 166, 169, 170
$tH (+q)$	$74^{+6}_{-11}^f$	Inclusive	$\tau\tau, WW, ZZ$	Multileptons	30.4	168, 169, 171
		Inclusive	$\gamma\gamma$	$\gamma\gamma+X$	0.2	169

Abbreviations: BR, branching ratio; EW, electroweak; NLO, next-to-leading order; NNLL, next-to-next-to-leading log; OS, opposite charge; PDF, parton distribution function; QCD, quantum chromodynamics; SS, same charge.

The different final states generated by the  $t\bar{t}$  and boson decays, and the channels explored, are listed in separate columns. For reference, the combined BR resulting from the  $W$  and  $Z$  boson BRs, and including the propagation of  $\tau$  leptonic decays, is given. The only exception is made for  $W$  and  $Z$  bosons generated after Higgs boson decay. The  $\sigma$  column quotes the prediction at  $\sqrt{s} = 13$  TeV and, with the exception of  $t\bar{t}W$  and  $t\bar{t}Z$ , includes fiducial cuts on the final-state leptons, photons, and jets. The quoted theory uncertainties include the PDF +  $\alpha_s$  and QCD scale choice uncertainties. The references for the experimental measurements are given in the last column. For the associated production with Higgs bosons, only a selected set of references for  $\sqrt{s} = 13$  TeV is given. The measurements cited in the last column may be made at different  $\sqrt{s}$  values, as specified in the footnotes below.

<sup>a</sup>The quoted fiducial  $t\bar{t}\gamma$  cross section is predicted at NLO QCD, as described in Reference 172, and corresponds to the selection of Reference 138.

<sup>b</sup>The quoted fiducial  $t\gamma$  cross section is predicted at NLO QCD accuracy (173) corresponding to the selection of Reference 144.

<sup>c</sup>Computed at NLO QCD and EW accuracy (175–177).

<sup>d</sup>Computed at NLO QCD accuracy in the five-flavor scheme (173) in the phase space of Reference 156.

<sup>e</sup>Computed at NLO including QCD and EW effects and NNLL QCD effects (174).

<sup>f</sup>Computed at NLO QCD accuracy (175).

a trilepton or a dilepton with the same electric charge. While full kinematics reconstruction is not possible with these final states, they have the advantage of higher purity. As in the  $t\bar{t}Z$  case, the measurements have typically been carried out using different categories (e.g., jet and  $b$  jet multiplicities), which enhance sensitivity to the signal and control the main background ( $t\bar{t}$  + jets, dibosons + heavy flavors, nonprompt leptons). The theoretical computation of these final states is challenging: It requires the proper handling of QCD and EW contributions to minimally describe the top quark decay at NLO, spin correlations, single-resonant and nonresonant contributions, and the emission of additional partons. Fixed-order NLO QCD + EW with complete off-shell effects has been computed in Reference 180, and NNLL contributions have been included only in the case of stable top quarks (181). The PS predictions, however, have NLO accuracy for the

production and are limited on-shell, with top quark decays at LO (175–177). Some effects (such as EW corrections) are more enhanced in  $t\bar{t}W$  than in  $t\bar{t}Z$ , making the former of great interest from the theoretical point of view. In Reference 182 it is estimated that NLO + PS cross sections, such as the one quoted in **Table 1**, fall short by 11–34% with respect to fixed-order calculations because of missing effects. It is therefore not surprising that, in general, the current  $t\bar{t}W$  measurements are approximately 20% higher than the SM prediction.

Experimentally, multilepton final states are very interesting as they comprise a multitude of different competing processes [e.g., top quark plus boson(s) or heavy flavors, four top quarks], which need to be controlled from data in dedicated selection regions. Additional contributions from wrong-charge measurements, conversions, and nonprompt leptons add to the overall challenge of these analyses. These effects are typically controlled with same-sign Z-like or looser lepton identification selections and add a 20–30% final uncertainty if not reduced with advanced MVA methods for lepton identification and isolation as well as event selection. The statistical analysis of signal and control regions by means of profiled maximum-likelihood techniques (183) is typically employed to constrain some of the backgrounds and systematic uncertainties. The most precise measurement of the  $t\bar{t}W$  cross section has a relative uncertainty of 7.5%, dominated by the statistical component and modeling of signal and background, most notably  $t\bar{t}H$ . This is illustrative of the interplay between  $t\bar{t}W$  and  $t\bar{t}H$ , which can only be improved in the future by a combined measurement of these two processes. Most systematic uncertainties are reduced in the charge asymmetry measurement, with  $\sigma_{t\bar{t}W^+}/\sigma_{t\bar{t}W^-} = 1.61^{+0.17}_{-0.16}$ , which is compatible with the SM prediction.

Although the observation of the Higgs boson (184, 185)—namely, in the  $H \rightarrow \gamma\gamma$  decay—is itself sensitive to  $y_t$ , which enters the production ( $gg \rightarrow H$ ) and decay loops, the direct measurement of  $t\bar{t}H$  offers the clearest line of sight to study  $y_t$ . Even if only a few direct measurements are cited in **Table 1**, typical Higgs boson analyses consider at least one  $t\bar{t}H$  category. The first observation of this process combines multilepton,  $b\bar{b}$ , and  $\gamma\gamma$  final states. With the exception of the latter, which can be reconstructed with high purity and mass resolution, these analyses rely significantly on the modeling of  $t\bar{t}+X$  and  $t+X$  backgrounds. Measurements made since the observation of a  $t\bar{t}H$  process (163, 166) show compatibility with an SM-like Higgs boson with an 11% relative uncertainty on  $y_t$  after full combination with other measurements (81, 82). Besides the interest in characterizing the  $t\bar{t}H$  coupling, this process is sensitive to both the Higgs boson triple self-coupling and a significant background in the measurement of the quartic Higgs boson self-coupling from  $HH$  processes. A more detailed review of the prospects is, however, out of scope, and the interested reader is referred to References 175 and 186. Searches for  $tHq$  have also been carried at the LHC. Although subdominant, this process is sensitive to the relative sign of  $y_t$  with respect to the  $WH$  coupling as the cross section is dominated by two contributions: one in which the Higgs boson couples to a space-like  $W$  boson and one in which it couples to the top quark. This yields  $\sigma_{tHq} \propto (c_f^2 - c_v)^2$ , with  $c_f$  and  $c_v$  the generalized (“scaled”) Higgs couplings to fermions and vector bosons, respectively. The production cross section almost cancels in the SM case and doubles in the BSM one. The results are compatible with the SM prediction.

### 3.4. Associated Production with Heavy Flavors

The production of  $t\bar{t}$  pairs and heavy flavor is a relevant test of pQCD and is important in measuring the dominant background for  $t\bar{t}H(\rightarrow b\bar{b})$  and  $t\bar{t}t\bar{t}$ . The difficulties in the analysis arise from the complex final state with several jets, two of which arise from gluon splitting and are soft and close to each other. Typically, jets are selected with  $p_T > 25\text{--}30$  GeV and  $|\eta| < 2.5$ , limiting the acceptance (<5%), and their flavor is identified by using MVAs with a combined efficiency that is currently <20% for  $t\bar{t}b\bar{b}$  and <10% for  $t\bar{t}c\bar{c}$ . The analyses are inclusive relative to the origin of the  $b\bar{b}$  system—that is, whether it stems from Higgs or Z boson decays produced in association with

the  $t\bar{t}$  system. The association of heavy-flavor jets from top quark decays is made using kinematic variables (e.g., mass-related or combined in an MVA discriminator), assuming  $B(t \rightarrow Wb) = 1$ . The production cross section is extracted from the multiplicity of  $b$  jets, a fit to the heavy-flavor discriminator of the additional jets, or a fit to a multiclassifier, depending on the analysis and final state. The  $t\bar{t}b$  and  $t\bar{t}c$  backgrounds need to be controlled with dedicated regions and profiled in fits.

The latest  $t\bar{t}b\bar{b}$  (187–189) and  $t\bar{t}c\bar{c}$  (190) measurements improve significantly over previous ones owing to higher statistics and better identification of heavy-flavored jets. Such improvements have been possible because of upgraded tracking systems in LHC Run 2 and state-of-the-art ML algorithms such as in References 50, 191, and 192. These algorithms are based on neural networks, which provide a more efficient way of detailing the intercorrelations of the constituents of a jet, the presence of secondary vertices, and other remnants of heavy-flavored hadron decays. The measurements have been carried in final states with zero, one, and two charged leptons. The main theoretical challenge stems from the multiscale nature of these processes, with large NLO corrections [ $\mathcal{O}(1.9)$ ] resulting in a large uncertainty of approximately 20% (193, 194). Thus, the latent difference of approximately 20% between experiment and theory has a reduced significance (1–2 $\sigma$ ) owing to the still-large uncertainties. Fiducial cross sections are measured with uncertainties  $\sim 9$ –30%, depending on the flavor and the final state, with the systematic uncertainty dominated by uncertainties in the calibration of flavor-tagging efficiencies, PS-related uncertainties, and the relative contribution of  $t\bar{t}b$  with respect to  $t\bar{t}b\bar{b}$ . PS-related uncertainties, as well as subdominant uncertainties on selection efficiencies and normalization, are reduced in the ratio  $\sigma(t\bar{t}b\bar{b})/\sigma(t\bar{t}q\bar{q})$ . Uncertainties from light flavor-tagging efficiency and relative contributions from one additional heavy-flavor jet remain nevertheless irreducible. Within the current ME + PS models, those that rely on PS only for high jet multiplicities tend to underestimate the rate of events with  $\geq 3b$ , indicating that either additional tuning or higher-order accuracy is needed. Among the differential measurements made in Reference 187, two of the most interesting are the opening angle between  $b\bar{b}$  pairs and their  $p_T$ . When  $b$  jets are chosen by proximity and in the purest channel (dilepton), the results disfavor 5FS fixed-order calculations with respect to the 4FS from Reference 195. In line with the other processes (e.g., as noted in Section 3.2), the 4FS generally better describes the rates and shapes of experimental distributions with respect to the 5FS. Other variables ( $H_T$ - and  $p_T$ -related) are, however, in general agreement for all models.

Further measurements with higher statistics and exploring possibly different jet algorithms, which can probe the softer phase space typically vetoed by the hard cuts, would be interesting.

### 3.5. Four Top Quark Production

At the LHC,  $t\bar{t}t\bar{t}$  production is the apex of top quark physics. This process has an expected cross section of  $\sigma_{t\bar{t}t\bar{t}}(\sqrt{s} = 13 \text{ TeV}) = 12^{+2}_-3 \text{ fb}$  at NLO QCD + EW accuracy (196), five orders of magnitude lower than the  $t\bar{t}$  production cross section. Several shortcomings in the modeling of the background need to be corrected for, with the modeling of  $t\bar{t}$  plus heavy flavors being the most crucial, given that in the signal region, four  $b$  jets and up to eight light jets from  $W$  boson decays are expected. Interestingly, the triple top quark process, despite its smaller cross section, contributes with a significant uncertainty, though it is not measured and lacks higher-order theory predictions. This type of final state also arises in several BSM scenarios (supersymmetry, simplified dark model, Type II Higgs doublet model), increasing the interest in  $t\bar{t}t\bar{t}$  production.

So far, experiments have searched for  $t\bar{t}t\bar{t}$  by covering the largest phase space possible using fully hadronic,  $1\ell$ ,  $2\ell$  OS,  $2\ell$  SS,  $3\ell$ , and  $4\ell$  final states. Currently, the best combined measurement comes from the ATLAS combination of all analyzed channels including  $1\ell$  and  $2\ell$  OS. With a corresponding 4.7 $\sigma$  significance,  $\sigma_{t\bar{t}t\bar{t}}(\sqrt{s} = 13 \text{ TeV}) = 24^{+7}_-6 \text{ fb}$  is compatible with the SM within

$2\sigma$  (197). The CMS experiment also finds evidence for the process after combining different channels, with a significance of  $4.0\sigma$  and measurement of  $\sigma_{t\bar{t}\bar{t}}(\sqrt{s} = 13 \text{ TeV}) = 17 \pm 5 \text{ fb}$  (198). For a detailed review of the selection, background control, and checks performed in these initial analyses, readers are referred to Reference 199. Despite the lower BR, the multilepton final-state  $2\ell\text{SS}$  and  $\geq 3\ell$  channels lead in sensitivity. Both the ATLAS and CMS Collaborations have published initial searches in these channels with the LHC Run 2 data set (200, 201) with observed  $4.3\sigma$  and  $2.6\sigma$  significance; the difference reflects the statistical fluctuations in the early stages of establishing this process at the LHC and the urgent need for more data. However, a reanalysis of the same data set, using improved lepton identification criteria and ML techniques, yielded the observation ( $>5\sigma$  significance) of the  $t\bar{t}\bar{t}$  process (202, 203). The improved measurements using the multilepton final states alone— $\sigma_{t\bar{t}\bar{t}}(\sqrt{s} = 13 \text{ TeV}) = 22.5^{+6.5}_{-5.5} \text{ fb}$  (ATLAS) and  $\sigma_{t\bar{t}\bar{t}}(\sqrt{s} = 13 \text{ TeV}) = 17.9^{+4.4}_{-4.1} \text{ fb}$  (CMS)—remain statistically limited and are in agreement with each other and the SM.

One of the most interesting results of these measurements, besides their sensitivity to BSM and anomalous couplings, is the measurement of  $y_t$  in a complementary manner to all of the methods referred to above. Neglecting interference terms, at LO,  $\sigma_{t\bar{t}\bar{t}} \propto |y_t/y_t^{\text{SM}}|^4$  (204). Including also the corresponding variation of the  $t\bar{t}H$  background, which contributes approximately 5% to the final limit,  $|y_t/y_t^{\text{SM}}| < 1.7$  is obtained at 95% CL (205). Further constraints on the Higgs boson propagator at dimension 6 from the so-called oblique  $\hat{H}$  parameter (206) can be obtained from  $t\bar{t}\bar{t}$  production. A parabolic variation of the cross section from  $\hat{H}$  is expected and has been used to obtain  $\hat{H} < 0.12$  at 95% CL (201). These limits are consistent with the expected sensitivity initially foreseen for the end of the High-Luminosity LHC (206).

### 3.6. Overview of Top Quark Production at the LHC

The sections above have reviewed the main results and reach of top quark physics in establishing the fundamental parameters of the theory. A simplified summary of results is provided in **Figure 5**, which displays the signal strength ( $\mu = \sigma/\sigma_{\text{theor}}$ ) of the different top quark production processes. The fine level of agreement with the SM is clear, and the expected increase in data and in the methodologies of the measurements updates the SM reference values to higher accuracy.

## 4. TOWARD THE DISCOVERY OF NEW PHYSICS THROUGH THE TOP QUARK FRONTIER

Given its properties, the top quark plays a central role in EW-scale dynamics, and it may be a window into the ultraviolet completeness of the SM. The abundant production of the top quark and its final-state diversity at the LHC make it appealing from the phenomenological point of view with a multitude of scenarios proposed—for instance, the  $Z'$  boson, compositeness, supersymmetry, leptoquarks, and vector-like quarks. The interested reader can find a more complete list of top quark-related searches in References 1, 13, and 14. The following section provides a short discussion of selected topics. The selection is motivated by the generic question of whether the top quark sector will probe the energy scale and flavor structure of potential new physics.

Two generic approaches can be taken toward discovery of new physics: a top-down approach, which maximizes the sensitivity of an analysis driven by a model that has solid theoretical grounding, and an inverse approach, in which a set of measured observables is analyzed for deviations from the SM that are compatible with a BSM contribution. The latter approach starts from well-defined observables and has the potential to map out from the data the BSM possibilities and their energy scale. One should, however, bear in mind that the theory of top quark production and decay is in development and lacks accuracy in several new phase-space regions that are being explored at the LHC.

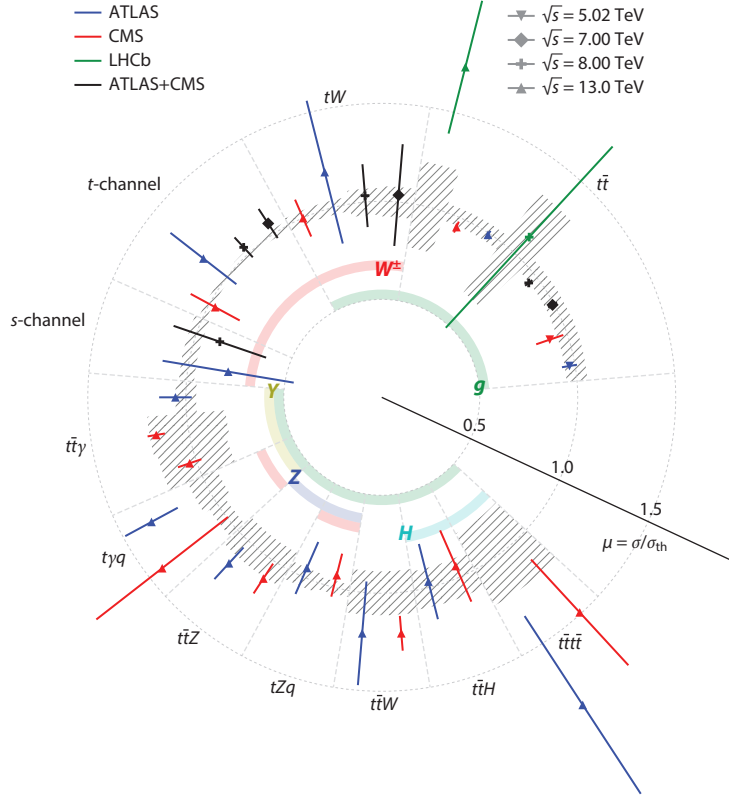


**Figure 5**

Pictorial summary of the signal strength from a representative set of cross section measurements of top quark production at the LHC, showing results at different  $\sqrt{s}$  values and from different experiments. Where available, the combined values by the LHC Top Physics Working Group (shown in *black*) have been used. Gray hatching indicates the uncertainty in the theory predictions. The error bars in the signal strengths do not include the propagation of the uncertainty on the denominators. The couplings of the top quark to the different bosons are marked by the colored arcs.

#### 4.1. Projecting the Scale of New Physics From Current Measurements

In the cautious, yet robust, bottom-up approach, the SM Lagrangian is extended with  $D = 6$  (or higher) operators ( $\mathcal{O}_i$ ), which introduce a rich set of phenomenological possibilities. The additional terms,  $\delta\mathcal{L} = \sum_i (C_i/\Lambda^2)\mathcal{O}_i + \dots$ , are suppressed by a BSM physics scale ( $\Lambda$ ) that is naturally heavier than any SM particle. The LHCTopWG has put forth a set of recommendations for the parameterization and interpretation of measurements for effective field theory (EFT) operators (207), which are based on the so-called Warsaw basis (208, 209) and define, among others, a baseline minimal-flavor-violation scenario to reduce the overwhelming number of four-fermion operators. The first approach considers the relevant operators to have a democratic contribution, with the data being used to constrain the relative hierarchies. In this way, the expansion in  $D = 6$  operator coefficients of an observable ( $O^k$ ) is written as

$$O^k = B_l^k + \frac{C_i}{\Lambda^2} S_i^k + \frac{C_i C_j}{\Lambda^4} S_{ij}^k + \dots, \quad 6.$$

- ① CMS,  $t\bar{t}$  + boosted  $Z/H$ \*
- ② CMS,  $t\bar{t}$ + $Z/W/H$ ,  $tZq$ ,  $tHq$
- ③ CMS, 4 top quarks
- ④ CMS,  $t\bar{t}\gamma$
- ⑤ CMS,  $tZq/t\bar{t}Z$
- ⑥ ATLAS,  $t\bar{t} \ell$ +jets boosted
- ⑦ ATLAS, top polarization

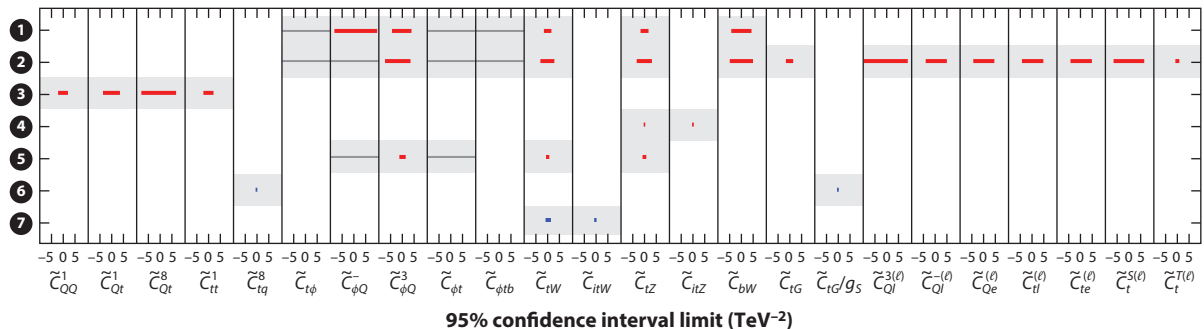


Figure 6

Summary of the 95% confidence level observed limits on the effective field theory Wilson coefficients of the dimension 6 operators related to interactions involving top quarks (215), as obtained by the ATLAS and CMS Collaborations for the following interactions: ①  $t\bar{t}$  + boosted  $Z/H$  (146), ②  $t\bar{t}$  +  $Z/W/H$ ,  $tZq$ ,  $tHq$  (216), ③ four top quarks (201), ④  $t\bar{t}\gamma$  (143), ⑤  $tZq/t\bar{t}Z$  (156), ⑥  $t\bar{t} \ell$  + jets boosted (83), and ⑦ top polarization (217). The results are reported as marginalized constraints, treating all Wilson coefficients that contribute to a given process as free parameters. The effect of a given Wilson coefficient is considered in multiple processes and across multiple bins of differential measurements. The results are reported as individual constraints assuming new physics contributions from one specific operator at a time. Interpretations use the Standard Model effective field theory (SMEFT) framework and the Warsaw basis and follow the LHC Top Physics Working Group (LHCTopWG) recommendations (207). Gray lines indicate operators included in the fit but with resulting limits outside  $[-10, 10]$ . Figure adapted from Reference 107 (CC BY 4.0).

where the SM contribution (for signal and background where relevant) is given by the first term ( $B_i^k$ ). With an estimation of the SM contribution, the linear ( $S_i^k$ ) and quadratic/interference ( $S_{ij}^k$ ) terms can be constrained from data to obtain limits on the Wilson coefficients ( $C_i$ ). Some examples can be found in References 146 and 210, and a summary from selected measurements and four-fermion operators is shown in **Figure 6**. By far, the most constraints (and the most stringent ones) come from the reinterpretation of associated productions, four top quarks, and inclusive cross section and spin correlation measurements. There are two interesting cases for future analysis. The first case uses simplified template cross sections (210): a concept developed for Higgs boson analysis, which consists of a set of optimized and mutually exclusive fiducial cross section definitions that are measurable by all experiments and facilitate the common interpretation. This concept, however, is not yet used in top quark analyses, in which a broader exploration and variety of measurements are still being performed, as described in Section 3. The second case is the one described in Reference 156, in which the sensitivity of the  $t\bar{t}Z$  and  $tZq$  final states to the relevant Wilson coefficients is optimized using MVA classifiers. After discriminating the SM processes from the backgrounds with a first classifier, a second set of binary classifiers further discriminates the EFT contributions from the SM-like signals. In the training, the interference term is also included because it affects the kinematics of the relevant variables. The main aim of this approach is to design observables with optimal sensitivity to new effects that arise from the targeted operators. A fit to these observables is then used to set limits on EFT operators. Several examples exist in the literature (211–214). As an illustration, **Figure 6** shows the limits obtained on top quark-related Wilson coefficients after marginalization. When performed globally (five-dimensionally in the

case of Reference 156), the constraints obtained from the data are looser (sometimes by a factor of three) as there may be competing effects from the different Wilson coefficients. In Reference 212 it is shown that after marginalization, and in the strong coupling limit [ $C_i \sim (4\pi)^2$ ], the scale of new physics is typically  $\Lambda \gtrsim 10$  TeV for the most stringent limits and after combining top quark with EW and Higgs boson data.

## 4.2. Chasing the BSM Tail From Asymmetries in the Data

The measurement of asymmetries in top quark production plays a particularly important role in BSM searches given the cancellation of several systematic variations.

One of the most interesting cases is related to the rapidity difference of the top quarks in  $t\bar{t}$  events ( $\Delta|y| = |y_t| - |y_{\bar{t}}|$ ) and its asymmetry defined as  $A_C = [\sigma(\Delta|y| > 0) - \sigma(\Delta|y| < 0)]/\sigma$ . Interest in  $A_C$  was raised after the Tevatron experiments reported a discrepancy between the data and SM predictions (218, 219). The dominance of the charge-symmetric gluon-gluon fusion and the fact that the asymmetry is generated at higher order from the interference of ISR and FSR diagrams ( $q\bar{q} \rightarrow t\bar{t} + g$ ) and box and Born diagrams ( $q\bar{q} \rightarrow t\bar{t}$ ) result in an overall small  $A_C = 0.95^{+0.05}_{-0.07}$  at NNLO QCD + NLO EW accuracy (220). Asymmetry is larger in some phase regions, such as  $m_{t\bar{t}} > 800$  GeV or forward top quark production, which enhances the relative contribution from  $q\bar{q}$  initial states. Evidence for this asymmetry was first shown in Reference 221. Inclusive and differential  $A_C$  measurements at the LHC have so far shown good agreement with the SM predictions and have been used to set limits either on EFT operators (see **Figure 6**) or on concrete BSM scenarios (e.g.,  $W'$  bosons, axigluons, color octets) (221–223). In the most extreme phase-space regions where  $A_C$  is enhanced [high  $m_{t\bar{t}}$ , low  $p_T(t\bar{t})$ , forward-rapidity regions], these are still statistically limited measurements. Additional enhancements to the asymmetry may be sought by requiring the presence of an additional jet or boson in the final state. The energy asymmetry in  $t\bar{t} + 1$  jet (224) and the charge asymmetry in  $t\bar{t}\gamma$  (225) events were recently measured to be compatible with the SM prediction.

Other asymmetry measurements test  $CP$  violation in the top quark sector. Sources of  $CP$  violation could arise from an anomalous  $CP$ -odd contribution to the chromoelectric dipole moment of the top quark, which would affect production, or anomalous  $tWb$  couplings, which would affect decay. Both would manifest as spin correlations. Beyond the measurement of the spin-density matrix and spin correlations (see Section 3.1), one can measure simple  $CP$ -odd observables based on the kinematics of the final and the reconstructed top and antitop quark kinematics. Such observables are usually called naive- $T$ -odd because they reverse sign under the operation that reverses the direction of momenta and spin without interchanging initial and final states. An example of such variables, defined for a single-lepton  $t\bar{t}$  final state, is  $O_3 = q_\ell \vec{p}_b^* \cdot (\vec{p}_t^* \times \vec{p}_{j_1}^*)$ , where the momenta of the bottom quark, charged lepton, and leading jet from the  $W \rightarrow q\bar{q}'$  decay are measured in the  $b\bar{b}$  reference frame, and  $q_\ell$  is the charge of the lepton. This observable is relatively easy to establish experimentally and is mostly affected by the purity of the  $t\bar{t}$  reconstruction algorithm. The measurement of the asymmetry  $A_{CP}(O_3) = [\sigma(O_3 > 0) - \sigma(O_3 < 0)]/\sigma$  cancels most experimental uncertainties, leaving a (currently statistically limited) constraint on  $CP$  violation in the top quark sector. The measurements made so far have a relative uncertainty of approximately 0.1% and show no  $CP$  violation (226, 227). The  $tWb$  vertex can also be tested for this purpose. In  $t\bar{t}$  events, the relative contributions from the different  $W$  boson helicities verify the SM predictions (228). The most precise measurement finds the fraction for right-handed  $W$  bosons to be  $f_R = 0.002 \pm 0.014$ , in agreement with the prediction  $f_R^{\text{SM}} = 0.0017 \pm 0.0001$  (229). However, the search for  $CP$ -violating contributions to the decay requires the measurement of a relative phase, as performed in single top quark events in Reference 230. The analysis of the relative phase between the amplitudes of the transversely and longitudinally polarized  $W$  bosons that recoil against

left-handed bottom quarks in single top quark events gives no indication of  $CP$  violation so far. Finally, although not specifically testing  $CP$  violation in the top quark sector,  $t\bar{t}$  events can be used as a source of  $b\bar{b}$  events to test  $CP$  asymmetries in heavy-flavor mixing and decay (231). By an appropriate combination of the charges of the leptons from semileptonic  $B$  hadron and  $W$  boson decays,  $t\bar{t}$  events offer the possibility of identifying the  $b$  charge at production and decay without resorting to standard flavor-tagging methods. With Run 1 data, the observed asymmetries are compatible with the residual ( $<10^{-4}$ ) SM predictions within the uncertainty range of 0.4% to 0.8% (232). Although statistically limited, systematics related to modeling of additional radiation and to the identification of soft leptons need to be improved to fully profit from higher-statistics data sets and to shed some light on the D0 observation of an anomalous same-sign dimuon charge asymmetry (233).

$CPT$  conservation can also be tested in the top quark sector. At the LHC this has (so far) been done by a measurement of the  $t - \bar{t}$  quark mass difference, which is a measurement of the asymmetry of  $m_t$ , as a function of the final-state lepton charge. The latest measurement is compatible with no  $\Delta m_t$ , within the 210-MeV statistically limited uncertainty (234). Compared with other  $CPT$ -related tests (1),  $m_t$  differences are still poorer and do not yet include tests of charge, width, or dipole moment differences.  $CPT$  violation may also encompass the violation of Lorentz symmetry. This could manifest in time-dependent  $t\bar{t}$  and single top quark production cross sections. So far, these possibilities have only been tested at the Tevatron with null results, within a 10% uncertainty (235).

### 4.3. Probing Flavor-Related Anomalies with Top Quarks

One of the most interesting tests in the top quark sector is that of flavor-changing neutral currents (FCNCs), which involve a neutral current ( $H, \gamma, Z, g$ ) and a modification of the quark flavor in either the production or the decay of a top quark. In the SM, FCNCs are highly suppressed with corresponding BRs  $\ll 10^{-11}$ , which cannot be observed at the LHC. Several BSM scenarios, however, predict sizable FCNCs in the top quark sector. Direct searches for such signatures are made in both production and decay. For a global summary of where these searches stand, readers are referred to **Figure 7** and the references cited therein (236–244). The current limits already probe the expected phase space of some models, such as the two Higgs doublet model, and are at the level of  $10^{-5}$  to  $10^{-3}$  depending on the signature. Because they are statistically limited, these are among the most obvious candidates for future improvements at the LHC.

Violations of other conservation laws—for instance, baryon number violation (BNV) and charged lepton flavor violation (CLFV)—are also subjects of interest in top quark physics. In a BNV scenario, a  $t \rightarrow \ell^+ \bar{b} \bar{c}$  decay could occur. Although an  $\mathcal{O}(10^{-27})$  BR is implied by the current limits on the proton lifetime, it can be significantly enhanced by some four-fermion operators. LHC Run 1 data have been used to set limits  $<0.15\%$  at 95% CL (246) on the BRs of such decays. Likewise, CLFV in the top quark sector has been searched for in  $t \rightarrow \ell^+ \ell^- q$  decays and in single top quark production in association with a  $\ell^+ \ell^-$  pair. These decays could be enhanced in the presence of a leptoquark or BSM four-fermion operators. Typical upper limits of BR(CPLV)  $< 10^{-6}$  at 95% CL (247, 248) are set.

Finally, tests of lepton universality can also be performed with  $t\bar{t}$  events by comparing the different BR( $W \rightarrow \ell\nu$ ). Final states with  $\tau$  leptons are particularly interesting given the slight tension from LEP measurements and recent measurements from LHCb and  $B$  factories (1). At the LHC,  $W \rightarrow \tau\nu$  decays are reconstructed using hadronic  $\tau$  decays (249) or from estimating the contribution from  $\tau \rightarrow \ell\nu\nu$  decays to leptonic observables in  $t\bar{t}$  events, assuming the leptonic  $\tau$  decay BR (250). Experimentally, the latter technique uses the fact that the final-state leptons from  $\tau$  decays tend to have a softer  $p_T$  spectrum and more displaced lepton production (higher  $d_{xy}$ ) than

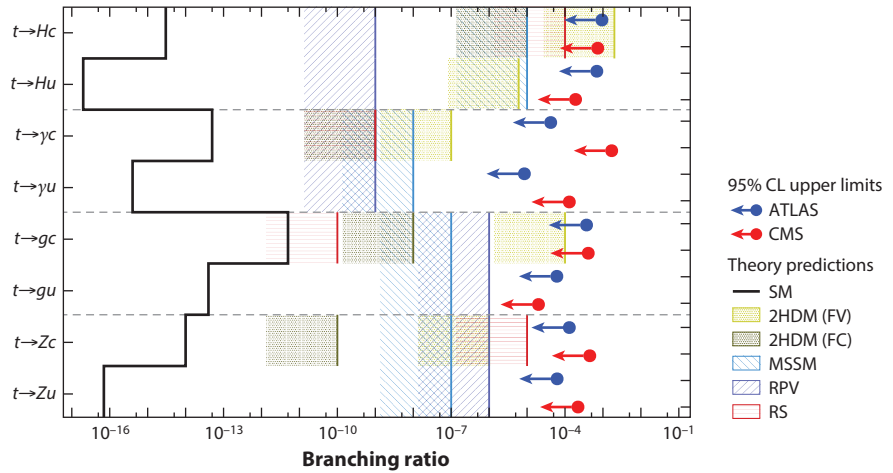


Figure 7

Summary of the current 95% confidence level limits on branching ratios of top quark decays via FCNCs to a neutral boson and a quark,  $t \rightarrow Xq$  ( $X = g, Z, \gamma, \text{ or } H$ ;  $q = u \text{ or } c$ ), observed by the ATLAS (236, 238, 240, 242) and CMS (237, 239, 241, 243, 244) Collaborations compared with the predictions of several new physics models (245). Each limit assumes that all other FCNC processes vanish. Abbreviations: FC, flavor conservation; FCNC, flavor-changing neutral current; FV, flavor violation; MSSM, minimal supersymmetric Standard Model; RPV,  $R$  parity violation; RS, Randall–Sundrum model; SM, Standard Model; 2HDM, two Higgs doublet model. ATLAS data from References 236 ( $t \rightarrow Hc$  and  $t \rightarrow Hu$ ), 238 ( $t \rightarrow \gamma c$  and  $t \rightarrow \gamma u$ ), 240 ( $t \rightarrow gc$  and  $t \rightarrow gu$ ), and 242 ( $t \rightarrow Zc$  and  $t \rightarrow Zu$ ). CMS data from References 237 ( $t \rightarrow Hc$  and  $t \rightarrow Hu$ ), 239 ( $t \rightarrow \gamma c$  and  $t \rightarrow \gamma u$ ), 241 ( $t \rightarrow gc$  and  $t \rightarrow gu$ ), 243 ( $t \rightarrow Zc$ ), and 244 ( $t \rightarrow Zu$ ). Figure adapted from Reference 107 (CC BY 4.0).

the ones that result directly from  $W$  boson decays. Despite its accompanying dependency on the calibration of the  $d_{xy}$  measurements, this technique has the advantage of improving the precision over the use of reconstructed hadronic  $\tau$  leptons because only electron and muon efficiencies, which cancel out in a ratio, are relevant. The resulting  $R(\tau/\mu) = B(W \rightarrow \tau\nu)/B(W \rightarrow \mu\nu) = 0.992 \pm 0.013$  in Reference 250 is consistent with lepton universality and improves significantly over the measurement performed at LEP.

## 5. SUMMARY AND OUTLOOK

Significant progress has been made during the 12 years that have passed since the top quark was “rediscovered” at the LHC (251, 252). The availability of large data samples from the LHC has been and will continue to be crucial to further advance progress in this top quark physics, which traverses the majority of the LHC program and remains a key frontier in the search for new phenomena. Future measurements of fundamental theory parameters as well as the search for deviations in the top quark sector will shape the legacy of the LHC on several fronts, including couplings of the Higgs boson, tests of  $CP$  violation, and the SM flavor structure.

Recent measurements and searches exploring new phase-space regions have become possible: Boosted top quarks, top quark production with vector or Higgs bosons, and processes with four top quarks are primary examples. On the experimental side, the ATLAS and CMS detectors will undergo a series of upgrades that will improve their measurement precision as they remain resilient

against the high pileup conditions foreseen for Phase 2 of the LHC while constantly improving their reconstruction, calibration, and analysis techniques. In the interim, theory has made giant steps to accompany the precision reach of the data. Several examples discussed in this review show that in this area, the SM is under active scrutiny; one such example is the achievement of NNLO QCD and NLO EW accuracy in  $t\bar{t}$  prediction during Run 2 of the LHC (253). Some critical future milestones in theory include higher-order accuracy in ME and PS generators, off-shell and nonresonant contributions to the processes of interest, and better modeling of nonperturbative effects such as color flow and bottom quark fragmentation. Fundamental parameters of the theory, such as  $m_t$ ,  $\alpha_S$ ,  $V_{tb}$ , and  $y_{t3}$ , are measured with relative uncertainties that are smaller than 0.5%, 1.8%, 2%, and 10%, respectively. Future improvements on these uncertainties have been illustrated, but they will only be useful as far as the precision of the accompanying theory predictions allows. These improvements also apply to searches for what potentially lies beyond the SM. Although an overall agreement between data and the current predictions has been found for the majority of the analyses made, the final word from the LHC will come only with the completion of the program by 2040.

## DISCLOSURE STATEMENT

This article reviews results mostly from three large LHC experiments; the author is a member of one of the three collaborations (CMS).

## ACKNOWLEDGMENTS

I thank the top quark physics group convenors of the ATLAS and CMS Collaborations, Marcel Vos, Andrea Knue, Jan Kieseleser, and Kai-Feng Chen, as well as the editor, for their valuable reviews and suggestions regarding the manuscript. The LHC Top Physics Working Group (LHCTopWG) is also acknowledged for making it possible to reuse some of the figures in this paper.

## LITERATURE CITED

1. Workman R, et al. *PTEP* 2022:083C01 (2022)
2. Peskin ME, Takeuchi T. *Phys. Rev. D* 46:381 (1992)
3. Degrandi G, et al. *J. High Energy Phys.* 1208:98 (2012)
4. Morrissey DE, et al. *Phys. Rep.* 515:1 (2012)
5. Aad G, et al. (ATLAS Collab.) *J. Instrum.* 3:S08003 (2008)
6. Chatrchyan S, et al. (CMS Collab.) *J. Instrum.* 3:S08004 (2008)
7. Alves AA Jr., et al. (LHCb Collab.) *J. Instrum.* 3:S08005 (2008)
8. Abe F, et al. (CDF Collab.) *Phys. Rev. Lett.* 74:2626 (1995)
9. Abachi S, et al. (D0 Collab.) *Phys. Rev. Lett.* 74:2632 (1995)
10. Campagnari C, Franklin M. *Rev. Mod. Phys.* 69:137 (1997)
11. Cristinziani M, Mulders M. *J. Phys. G* 44:063001 (2017)
12. Giammanco A, Schwienhorst R. *Rev. Mod. Phys.* 90:035001 (2018)
13. ATLAS Collab. Top-quark physics. *CERN*. <https://twiki.cern.ch/twiki/bin/view/AtlasPublic/TopPublicResults> (2023)
14. CMS Collab. Top physics publications. *CERN*. <http://cms-results.web.cern.ch/cms-results/public-results/publications/TOP/index.html> (2023)
15. LHCb Collab. Publications of the QCD, Electroweak and Exotica Working Group. *CERN*. <https://lhcbproject.web.cern.ch/Publications/LHCbProjectPublic/SummaryEE.html> (2023)
16. ATLAS/CMS Collab. LHCTopWG—LHC Top Physics Working Group. *CERN*. <https://twiki.cern.ch/twiki/bin/view/LHCPhysics/LHCTopWG> (2023)

17. ATLAS/CDF/CMS/D0 Collab. Report ATLAS-CONF-2014-008/CDF-NOTE-11071/CMS-PAS-TOP-13-014/D0-NOTE-6416/FERMILAB-TM-2582-E, CERN/Fermilab, Geneva/Batavia, IL (2014)
18. Bigi I, et al. *Phys. Lett. B* 181:157 (1986)
19. Ferrario Ravasio S, et al. *Eur. Phys. J. C* 78:458 (2018). Addendum. *Eur. Phys. J. C* 79:859 (2019)
20. Hoang AH. *Annu. Rev. Nucl. Part. Sci.* 70:225 (2020)
21. Cowan G. *Statistical Data Analysis*. Oxford, UK: Oxford Univ. Press (1998)
22. ATLAS/CMS Collab. Particle level objects and pseudo-top-quark definitions. CERN. <https://twiki.cern.ch/twiki/bin/view/LHCPhysics/ParticleLevelTopDefinitions> (2016)
23. CMS Collab. Report CERN-CMS-NOTE-2017-004, CERN, Geneva (2017)
24. Argyropoulos S, Sjöstrand T. *J. High Energy Phys.* 1411:43 (2014)
25. Christiansen JR, Skands PZ. *J. High Energy Phys.* 1508:3 (2015)
26. Gieseke S, et al. *Eur. Phys. J. C* 72:2225 (2012)
27. Aad G, et al. (ATLAS Collab.) *Eur. Phys. J. C* 79:1028 (2019). Erratum. *Eur. Phys. J. C* 80:1092 (2020)
28. Aad G, et al. (ATLAS Collab.) *J. High Energy Phys.* 2304:80 (2023)
29. Tumasyan A, et al. (CMS Collab.) *Phys. Rev. D* 104:092013 (2021)
30. Sirunyan AM, et al. (CMS Collab.) *Phys. Rev. D* 103:052008 (2021)
31. Aaboud M, et al. (ATLAS Collab.) *J. High Energy Phys.* 1908:33 (2019)
32. Aaboud M, et al. (ATLAS Collab.) *Eur. Phys. J. C* 78:847 (2018)
33. Sirunyan AM, et al. (CMS Collab.) *Phys. Rev. D* 98:092014 (2018)
34. Aad G, et al. (ATLAS Collab.) *Phys. Rev. D* 106:032008 (2022)
35. CMS Collab. Report CMS-PAS-TOP-18-012, CERN, Geneva (2021)
36. Sirunyan AM, et al. (CMS Collab.) *Eur. Phys. J. C* 79:123 (2019)
37. Amoroso S, et al. *Comput. Softw. Big Sci.* 5:12 (2021)
38. Cacciari M, et al. *J. High Energy Phys.* 0804:063 (2008)
39. Cacciari M, et al. *Eur. Phys. J. C* 72:1896 (2012)
40. Aad G, et al. (ATLAS Collab.) *Eur. Phys. J. C* 81:689 (2021)
41. Khachatryan V, et al. (CMS Collab.) *J. Instrum.* 12:P02014 (2017)
42. Sjöstrand T, et al. *Comput. Phys. Commun.* 191:159 (2015)
43. Bahr M, et al. *Eur. Phys. J. C* 58:639 (2008)
44. CMS Collab. Report CMS-PAS-JME-13-001, CERN, Geneva (2014)
45. ATLAS Collab. arXiv:2303.17312 [hep-ex] (2023)
46. Sirunyan AM, et al. (CMS Collab.) *Eur. Phys. J. C* 78:891 (2018). Erratum. *Eur. Phys. J. C* 82:323 (2022)
47. CMS Collab. arXiv:2211.01456 [hep-ex] (2022)
48. Aaboud M, et al. (ATLAS Collab.) *Eur. Phys. J. C* 79:290 (2019)
49. Aad G, et al. (ATLAS Collab.) *Eur. Phys. J. C* 79:970 (2019)
50. Sirunyan AM, et al. (CMS Collab.) *J. Instrum.* 13:P05011 (2018)
51. LHCb Collab. *J. Instrum.* 10:P06013 (2015)
52. Stewart I, et al. *Phys. Rev. Lett.* 105:092002 (2010)
53. Stewart I, et al. *J. High Energy Phys.* 1511:72 (2015)
54. Sirunyan AM, et al. (CMS Collab.) *Phys. Rev. Lett.* 124:202001 (2020)
55. Aaboud M, et al. (ATLAS Collab.) *Eur. Phys. J. C* 77:466 (2017)
56. Sirunyan AM, et al. (CMS Collab.) *J. Instrum.* 12:P10003 (2017)
57. Bertolini D, et al. *J. High Energy Phys.* 1410:59 (2014)
58. ATLAS Collab. Technical Design Report CERN-LHCC-2013-018, CERN, Geneva (2013)
59. CMS Collab. Technical Design Report CERN-LHCC-2020-004, CERN, Geneva (2020)
60. CMS Collab. Technical Design Report CERN-LHCC-2021-007, CERN, Geneva (2021)
61. ATLAS Collab. Technical Design Report CERN-LHCC-2015-020, CERN, Geneva (2015)
62. CMS Collab. Technical Design Report CERN-LHCC-2015-010, CERN, Geneva (2015)
63. Kiyoyama Y, et al. *Eur. Phys. J. C* 60:375 (2009)
64. Sumino Y, Yokoyama H. *J. High Energy Phys.* 1009:34 (2010). Erratum. *J. High Energy Phys.* 1606:37 (2016)
65. Czakon M, et al. *Phys. Rev. Lett.* 110:252004 (2013)

66. Catani S, et al. *J. High Energy Phys.* 1907:100 (2019)
67. ATLAS Collab. arXiv:2207.01354 [hep-ex] (2022)
68. Sirunyan AM, et al. (CMS Collab.) *J. High Energy Phys.* 1803:115 (2018)
69. ATLAS/CMS Collab. Report CERN-EP-2021-222, CERN, Geneva (2022)
70. Aad G, et al. (ATLAS Collab.) *Eur. Phys. J. C* 80:528 (2020)
71. Sirunyan AM, et al. (CMS Collab.) *Eur. Phys. J. C* 79:368 (2019)
72. Aaij R, et al. (LHCb Collab.) *Phys. Lett. B* 767:110 (2017)
73. Aaij R, et al. (LHCb Collab.) *J. High Energy Phys.* 1808:174 (2018)
74. Sirunyan AM, et al. (CMS Collab.) *Phys. Rev. Lett.* 119:242001 (2017)
75. Sirunyan AM, et al. (CMS Collab.) *Phys. Rev. Lett.* 125:222001 (2020)
76. Sirunyan AM, et al. (CMS Collab.) *Eur. Phys. J. C* 80:658 (2020)
77. Aad G, et al. (ATLAS Collab.) *J. High Energy Phys.* 1911:150 (2019)
78. CMS Collab. arXiv:2207.02270 [hep-ex] (2022)
79. Sirunyan AM, et al. (CMS Collab.) *Phys. Lett. B* 803:135263 (2020)
80. Sirunyan AM, et al. (CMS Collab.) *Phys. Rev. D* 102:092013 (2020)
81. ATLAS Collab. *Nature* 607:52 (2022). Erratum. *Nature* 612:E24 (2022)
82. CMS Collab. *Nature* 607:60 (2022)
83. Aad G, et al. (ATLAS Collab.) *J. High Energy Phys.* 2206:63 (2022)
84. Khachatryan V, et al. (CMS Collab.) *Phys. Rev. D* 94:052006 (2016)
85. Sirunyan AM, et al. (CMS Collab.) *J. High Energy Phys.* 1902:149 (2019)
86. Denner A, et al. *Phys. Rev. Lett.* 106:052001 (2011)
87. Bevilacqua G, et al. *J. High Energy Phys.* 1102:83 (2011)
88. Denner A, Pellen M. *J. High Energy Phys.* 1608:155 (2016)
89. Behring A, et al. *Phys. Rev. Lett.* 123:082001 (2019)
90. Czakon M, et al. *J. High Energy Phys.* 2105:212 (2021)
91. Denner A, et al. *Nucl. Phys. B* 560:33 (1999)
92. Mazzitelli J, et al. *Phys. Rev. Lett.* 127:062001 (2021)
93. Mazzitelli J, et al. *J. High Energy Phys.* 2204:79 (2022)
94. Aaboud M, et al. (ATLAS Collab.) *Eur. Phys. J. C* 77:804 (2017)
95. Aaboud M, et al. (ATLAS Collab.) *Phys. Rev. Lett.* 121:152002 (2018)
96. Catani S, Webber BR, Marchesini G. *Nucl. Phys. B* 349:635 (1991)
97. ATLAS Collab. arXiv:2209.07874 [hep-ex] (2022)
98. Aad G, et al. (ATLAS Collab.) *Eur. Phys. J. C* 79:1017 (2019)
99. Afik Y, et al. *Eur. Phys. J. Plus* 136:907 (2021)
100. Bernreuther W, et al. *J. High Energy Phys.* 1512:26 (2015)
101. Severi C, et al. *Eur. Phys. J. C* 82:285 (2022)
102. Brandenburg A, Si ZG, Uwer P. *Phys. Lett. B* 539:235 (2002)
103. Aaboud M, et al. (ATLAS Collab.) *J. High Energy Phys.* 1703:113 (2017)
104. Sirunyan AM, et al. (CMS Collab.) *Phys. Rev. D* 100:072002 (2019)
105. Aaboud M, et al. (ATLAS Collab.) *Eur. Phys. J. C* 80:754 (2020)
106. Khachatryan V, et al. (CMS Collab.) *Phys. Rev. D* 93:052007 (2016)
107. ATLAS/CMS Collab. LHCTopWG summary plots. CERN. <https://twiki.cern.ch/twiki/bin/view/LHCPhysics/LHCTopWGSummaryPlots> (2023)
108. Aad G, et al. (ATLAS Collab.) *Phys. Lett. B* 756:228 (2016)
109. ATLAS Collab. arXiv:2209.08990 [hep-ex] (2022)
110. Khachatryan V, et al. (CMS Collab.) *J. High Energy Phys.* 1609:27 (2016)
111. Kant P, et al. *Comput. Phys. Commun.* 191:74 (2015)
112. Aliev M, et al. *Comput. Phys. Commun.* 182:1034 (2011)
113. Aaboud G, et al. (ATLAS/CMS Collab.) *J. High Energy Phys.* 1905:88 (2019)
114. Aaboud G, et al. (ATLAS Collab.) *J. High Energy Phys.* 1704:86 (2017)
115. Sirunyan AM, et al. (CMS Collab.) *Phys. Lett. B* 800:135042 (2020)
116. Berger EL, Gao J, Zhu HX. *J. High Energy Phys.* 1711:158 (2017)

117. Brucherseifer M, et al. *Phys. Lett. B* 736:58 (2014)
118. Aaboud M, et al. (ATLAS Collab.) *Eur. Phys. J. C* 77:531 (2017)
119. Sirunyan AM, et al. (CMS Collab.) *Eur. Phys. J. C* 80:370 (2020)
120. Schwienhorst R, et al. *Phys. Rev. D* 83:034019 (2011)
121. Aaboud M, et al. (ATLAS Collab.) *J. High Energy Phys.* 1704:124 (2017)
122. Khachatryan V, et al. (CMS Collab.) *J. High Energy Phys.* 1604:73 (2016)
123. Aad G, et al. (ATLAS Collab.) *J. High Energy Phys.* 1604:23 (2016)
124. Kidonakis N. *Phys. Rev. D* 82:054018 (2010)
125. Kidonakis N. arXiv:1311.0283 [hep-ph] (2014)
126. Frixione S, et al. *J. High Energy Phys.* 0807:029 (2008)
127. Belyaev AS, Boos EE, Dudko LV. *Phys. Rev. D* 59:075001 (1999)
128. White CD, et al. *J. High Energy Phys.* 0911:074 (2009)
129. Tait T. *Phys. Rev. D* 61:034001 (1999)
130. Aaboud M, et al. (ATLAS Collab.) *J. High Energy Phys.* 1801:63 (2018)
131. CMS Collab. arXiv:2208.00924 [hep-ex] (2022)
132. Tumasyan A, et al. (CMS Collab.) *J. High Energy Phys.* 2111:111 (2021)
133. Aaboud M, et al. (ATLAS Collab.) *Eur. Phys. J. C* 78:186 (2018)
134. Ježo T, et al. *Eur. Phys. J. C* 76:691 (2016)
135. Sirunyan AM, et al. (CMS Collab.) *Phys. Lett. B* 808:135609 (2020)
136. Khachatryan V, et al. (CMS Collab.) *Phys. Lett. B* 736:33 (2014)
137. Aad G, et al. (ATLAS Collab.) *Phys. Rev. D* 91:072007 (2015)
138. Aaboud M, et al. (ATLAS Collab.) *J. High Energy Phys.* 1711:86 (2017)
139. Aaboud M, et al. (ATLAS Collab.) *Eur. Phys. J. C* 79:382 (2019)
140. Sirunyan AM, et al. (CMS Collab.) *J. High Energy Phys.* 1710:6 (2017)
141. Tumasyan A, et al. (CMS Collab.) *J. High Energy Phys.* 2112:180 (2021)
142. Aad G, et al. (ATLAS Collab.) *J. High Energy Phys.* 2009:49 (2020)
143. Tumasyan A, et al. (CMS Collab.) *J. High Energy Phys.* 2205:91 (2022)
144. Sirunyan AM, et al. (CMS Collab.) *Phys. Rev. Lett.* 121:221802 (2018)
145. ATLAS Collab. arXiv:2302.01283 [hep-ex] (2023)
146. CMS Collab. arXiv:2208.12837 [hep-ex] (2022)
147. Aad G, et al. (ATLAS Collab.) *J. High Energy Phys.* 1511:172 (2015)
148. Khachatryan V, et al. (CMS Collab.) *J. High Energy Phys.* 1601:96 (2016)
149. Aaboud M, et al. (ATLAS Collab.) *Phys. Rev. D* 99:072009 (2019)
150. Aaboud M, et al. (ATLAS Collab.) *Eur. Phys. J. C* 77:40 (2017)
151. Aad G, et al. (ATLAS Collab.) *Eur. Phys. J. C* 81:737 (2021)
152. Chatrchyan S, et al. (CMS Collab.) *Phys. Rev. Lett.* 110:172002 (2013)
153. Khachatryan V, et al. (CMS Collab.) *Eur. Phys. J. C* 74:3060 (2014)
154. Sirunyan AM, et al. (CMS Collab.) *J. High Energy Phys.* 1808:11 (2018)
155. Sirunyan AM, et al. (CMS Collab.) *J. High Energy Phys.* 2003:56 (2020)
156. Tonon N, et al. (CMS Collab.) *J. High Energy Phys.* 2112:83 (2021)
157. Aaboud M, et al. (ATLAS Collab.) *Phys. Lett. B* 780:557 (2018)
158. Aad G, et al. (ATLAS Collab.) *J. High Energy Phys.* 2007:124 (2020)
159. Sirunyan AM, et al. (CMS Collab.) *Phys. Lett. B* 779:358 (2018)
160. Sirunyan AM, et al. (CMS Collab.) *Phys. Rev. Lett.* 122:132003 (2019)
161. CMS Collab. arXiv:2208.06485 [hep-ex] (2022)
162. Aaboud M, et al. (ATLAS Collab.) *Phys. Rev. D* 97:072016 (2018)
163. Aaboud M, et al. (ATLAS Collab.) *Phys. Lett. B* 784:173 (2018)
164. Aad G, et al. (ATLAS Collab.) *J. High Energy Phys.* 2206:97 (2022)
165. Sirunyan AM, et al. (CMS Collab.) *J. High Energy Phys.* 1903:26 (2019)
166. Sirunyan AM, et al. (CMS Collab.) *Phys. Rev. Lett.* 120:231801 (2018)
167. Aaboud M, et al. (ATLAS Collab.) *Phys. Rev. D* 97:072003 (2018)
168. Sirunyan AM, et al. (CMS Collab.) *Eur. Phys. J. C* 81:378 (2021)

169. Aad G, et al. (ATLAS Collab.) *Phys. Rev. Lett.* 125:061802 (2020)
170. Sirunyan AM, et al. (CMS Collab.) *Phys. Rev. Lett.* 125:061801 (2020)
171. Sirunyan AM, et al. (CMS Collab.) *Phys. Rev. D* 99:092005 (2019)
172. Melnikov K, et al. *Phys. Rev. D* 83:074013 (2011)
173. Alwall J, et al. *J. High Energy Phys.* 1407:79 (2014)
174. Kulesza A, et al. *Eur. Phys. J. C* 80:428 (2020)
175. de Florian D, et al., eds. (LHC Higgs Cross Section Working Group.) *Handbook of LHC Higgs Cross Sections: 4. Deciphering the Nature of the Higgs Sector.* Geneva: CERN (2017)
176. Frixione S, et al. *J. High Energy Phys.* 1506:184 (2015)
177. Frederix R, et al. *J. High Energy Phys.* 1807:185 (2018). Erratum. *J. High Energy Phys.* 2111:85 (2021)
178. Schulze M, Soreq Y. *Eur. Phys. J. C* 76:466 (2016)
179. Aguilar-Saavedra JA, et al. *J. High Energy Phys.* 1404:188 (2014)
180. Denner A, Pelliccioli G. *Eur. Phys. J. C* 81:354 (2021)
181. Broggio A, et al. *J. High Energy Phys.* 1908:39 (2019)
182. Bevilacqua G, et al. *Phys. Rev. D* 105:014018 (2022)
183. ATLAS/CMS Collab., LHC Higgs Comb. Group. Report CMS-NOTE-2011-005/ATL-PHYS-PUB-2011-011, CERN, Geneva (2011)
184. Aad G, et al. (ATLAS Collab.) *Phys. Lett. B* 710:49 (2012)
185. Chatrchyan S, et al. (CMS Collab.) *Phys. Lett. B* 716:30 (2012)
186. Dainese A, et al., eds. *Physics of the HL-LHC, and Perspectives at the HE-LHC.* Geneva: CERN (2019)
187. Aaboud M, et al. (ATLAS Collab.) *J. High Energy Phys.* 1904:46 (2019)
188. Sirunyan AM, et al. (CMS Collab.) *Phys. Lett. B* 803:135285 (2020)
189. Sirunyan AM, et al. (CMS Collab.) *J. High Energy Phys.* 2007:125 (2020)
190. Sirunyan AM, et al. (CMS Collab.) *Phys. Lett. B* 820:136565 (2021)
191. ATLAS Collab. arXiv:2211.16345 [physics.data-an] (2022)
192. Tumasyan A, et al. (CMS Collab.) *J. Instrum.* 17:P03014 (2022)
193. Denner A, et al. *Phys. Rev. D* 104:056018 (2021)
194. Bevilacqua G, et al. *Phys. Rev. D* 107:014028 (2023)
195. Garzelli MV, et al. *J. High Energy Phys.* 1503:83 (2015)
196. Ježo T, Kraus M. *Phys. Rev. D* 105:114024 (2022)
197. Aad G, et al. (ATLAS Collab.) *J. High Energy Phys.* 2111:118 (2021)
198. CMS Collab. arXiv:2303.03864 [hep-ex] (2023)
199. Blekman F, et al. *Universe* 8:638 (2022)
200. Aad G, et al. (ATLAS Collab.) *Eur. Phys. J. C* 80:1085 (2020)
201. Sirunyan AM, et al. (CMS Collab.) *J. High Energy Phys.* 1911:82 (2019)
202. ATLAS Collab. arXiv:2303.15061 [hep-ex] (2023)
203. CMS Collab. Report CMS-PAS-TOP-22-013, CERN, Geneva (2023)
204. Cao QH, et al. *Phys. Rev. D* 95:053004 (2017)
205. Sirunyan AM, et al. (CMS Collab.) *Eur. Phys. J. C* 80:75 (2020)
206. Englert C, et al. *J. High Energy Phys.* 1909:41 (2019)
207. Barducci D, et al. Report CERN-LPCC-2018-01, CERN, Geneva (2018)
208. Aguilar-Saavedra JA. *Nucl. Phys. B* 812:181 (2009)
209. Zhang C, Willenbrock S. *Phys. Rev. D* 83:034006 (2011)
210. ATLAS Collab. Report ATL-PHYS-PUB-2022-037, CERN, Geneva (2022)
211. Brivio I, et al. *J. High Energy Phys.* 2002:131 (2020)
212. Ellis J, et al. *J. High Energy Phys.* 2104:279 (2021)
213. Ethier J, et al. *J. High Energy Phys.* 2111:89 (2021)
214. Miralles V, et al. *J. High Energy Phys.* 2202:32 (2022)
215. Aguilar Saavedra JA, et al. arXiv:1802.07237 [hep-ph] (2018)
216. Sirunyan AM, et al. (CMS Collab.) *J. High Energy Phys.* 2103:95 (2021)
217. Aad G, et al. (ATLAS Collab.) *J. High Energy Phys.* 2211:40 (2022)
218. Aaltonen T, et al. (CDF Collab.) *Phys. Rev. D* 87:092002 (2013)

219. Abazov VM, et al. (D0 Collab.) *Phys. Rev. D* 90:072011 (2014)
220. Czakon M, et al. *Phys. Rev. D* 98:014003 (2018)
221. ATLAS Collab. arXiv:2208.12095 [hep-ex] (2022)
222. Aaboud M, et al. (ATLAS/CMS Collab.) *J. High Energy Phys.* 1804:33 (2018)
223. CMS Collab. arXiv:2208.02751 [hep-ex] (2022)
224. Aad G, et al. (ATLAS Collab.) *Eur. Phys. J. C* 82:374 (2022)
225. ATLAS Collab. 2212.10552 [hep-ex] (2022)
226. CMS Collab. arXiv:2205.07434 [hep-ex] (2022)
227. CMS Collab. arXiv:2205.02314 [hep-ex] (2022)
228. Aad G, et al. CMS/ATLAS Collab. *J. High Energy Phys.* 2008:51 (2020)
229. ATLAS Collab. arXiv:2209.14903 [hep-ex] (2022)
230. Aaboud M, et al. (ATLAS Collab.) *J. High Energy Phys.* 1712:17 (2017)
231. Gedalia O, et al. *Phys. Rev. Lett.* 110:232002 (2013)
232. Aaboud M, et al. (ATLAS Collab.) *J. High Energy Phys.* 1702:71 (2017)
233. Abazov VM, et al. (D0 Collab.) *Phys. Rev. D* 82:032001 (2010)
234. Chatrchyan S, et al. (CMS Collab.) *Phys. Lett. B* 770:50 (2017)
235. Abazov VM, et al. (D0 Collab.) *Phys. Rev. Lett.* 108:261603 (2012)
236. ATLAS Collab. arXiv:2208.11415 [hep-ex] (2022)
237. Tumasyan A, et al. (CMS Collab.) *Phys. Rev. Lett.* 129:032001 (2022)
238. Aad G, et al. (ATLAS Collab.) *Phys. Lett. B* 842:137379 (2023)
239. Khachatryan V, et al. (CMS Collab.) *J. High Energy Phys.* 1604:35 (2016)
240. Aad G, et al. (ATLAS Collab.) *Eur. Phys. J. C* 82:334 (2022)
241. Khachatryan V, et al. (CMS Collab.) *J. High Energy Phys.* 1702:28 (2017)
242. ATLAS Collab. Report ATLAS-CONF-2021-049, CERN, Geneva (2021)
243. CMS Collab. Report CMS-PAS-TOP-17-017, CERN, Geneva (2017)
244. Sirunyan AM, et al. *J. High Energy Phys.* 1707:3 (2017)
245. Agashe K, et al. arXiv:1311.2028 [hep-ph] (2013)
246. Chatrchyan S, et al. (CMS Collab.) *Phys. Lett. B* 731:173 (2014)
247. ATLAS Collab. Report ATLAS-CONF-2023-001, CERN, Geneva (2023)
248. Tumasyan A, et al. (CMS Collab.) *J. High Energy Phys.* 2206:82 (2022)
249. Tumasyan A, et al. (CMS Collab.) *Phys. Rev. D* 105:072008 (2022)
250. ATLAS Collab. *Nat. Phys.* 17:813 (2021)
251. Aad G, et al. (ATLAS Collab.) *Eur. Phys. J. C* 71:1577 (2011)
252. Khachatryan V, et al. (CMS Collab.) *Phys. Lett. B* 695:424 (2011)
253. Czakon M, et al. *J. High Energy Phys.* 1710:186 (2017)